Doctoral Dissertation

Studies on Low Frequency AC Transmission System Using Modular Multilevel Matrix Converter Based Virtual Synchronous Generator Control

（モジュラーマルチレベルマトリックスコンバータにおける仮想同期発電機制御を適用した低周波交流送電システムに関する研究）

Al-Tameemi Mustafa Jawad Kadhim

June, 2020

Division of Electrical, Electronic
and Information Engineering
Graduate School of Engineering
Osaka University

Abstract

This thesis studies the operation, control, and applications of a low frequency ac transmission (LFAC) system driven by a modular multilevel matrix converter (M3C) and controlled using a virtual synchronous generator (VSG) concept. The LFAC system is receiving noticeable attention to be an alternative transmission technology solution along with nominal frequency (50 Hz and/or 60 Hz) high voltage ac (HVAC) transmission technology and high voltage direct current (HVDC) transmission technology.

In this work, the LFAC system, the M3C and the VSG controller are introduced altogether to provide a combination of technical advantages, such as; 1) transmission distance can be increased compared to the HVAC system; 2) more reliable response against fault compared to the HVDC system. The M3C is expected to be the next ac/ac generation converter due to the technical advantages such as lower harmonics, higher power factor and quick response. These advantages make the M3C employment promising in the LFAC power systems.

Application of VSG control is proposed to enable proper power-sharing, to provide synchronization of each terminal and frequency stabilization. The VSG controller provides power synchronization between frequency converter terminals in an autonomous manner with virtual inertia by emulating the equivalent swing equation of a synchronous generator (SG). This scheme is meant to present a new control scheme for the LFAC transmission system in order to extend the point-to-point concept to form a multi-terminal LFAC (MT-LFAC) system, which has not yet been reported before in literature. This configuration is also meant for applications that require interconnection of remote power systems operating in nominal frequency via LFAC transmission lines.

A novel control scheme of the remote ac grid-side M3C, which makes both interactions with the LFAC system and the remote ac grid behave like a synchronous generator using a dual VSG control scheme is studied. This control scheme can enhance the frequency regulation in the remote ac grid, which the existing control schemes cannot provide.

This dissertation is organized as follows:

In Chapter 1, it gives a brief idea of the current situation of the existing power grid. The feasibility of the current transmission technologies, power electronic converters, and associated control schemes to respond to the drastic change in the power grid is discussed. The discussion is then translated into the objectives of this study.

In Chapter 2, it compares the existing transmission technologies against the proposed LFAC system, and reason for choosing the LFAC system in this work. Furthermore, the M3C configuration, topology and control are described. Besides, the VSG concept and its adaptation to the M3C-LFAC system is explained.

In Chapter 3, the M3C-LFAC system with the VSG controller to form and operate a point-to-point configuration is studied. The VSG droop controller based on conventional and reversed one is applied for this configuration. Case studies included a power flow from one point to the other following a command change and a direction of power flow change scenario.

In Chapter 4, a multiterminal-LFAC (MT-LFAC) configuration is formed by extending the point-to-point M3C-LFAC configuration using VSG control. This configuration and its controller are studied. Moreover, a control technique for sharing the reactive power of an MT-LFAC system using an automatic voltage regulator (AVR) and automatic reactive power regulator (AQR) is investigated and applied in the system. Issues related to the design of the LFAC system are emerged and solved, such as the problem of the low *X/R* ratio when selecting the parameters of the LFAC transmission. A stator virtual impedance for improving the *X/R* ratio of the LFAC system is proposed. Autonomous operation is established based on the frequency restoration mode (FRM) for the governor part of the VSG controller. This frequency restoration mode relies on the online output power instead of a predefined command. Three dynamic scenarios are simulated to fully validate this configuration and its proposed control schemes. Two case studies were applied based on selecting a commanded mode (CM) or FRM for operating the terminals, and a third case study to ensure that the VSG can guarantee smooth and stable operation when transitioning between those operating modes.

In Chapter 5, a dual VSG controller is employed for each M3Cs in the point-to-point LFAC configuration. This system is connected to a remote ac grid in order to enhance its frequency regulation. This system can increase the total inertia of a remote ac grid in which conventional current controllers cannot provide. Dynamic cases include; a load changing and an occurrence of a fault. The target of this work is to compare the conventional controller for the M3C converter with a dual VSG-based M3C on both LFAC and grid sides in terms of providing a frequency regulation support to a remote ac grid.

In Chapter 6, conclusions are presented and some suggestions for the LFAC as well as the M3C need to be considered in the future are discussed.

Table of Contents

Chapter 1
Introduction

In this chapter, a general background about the existed transmission systems, power control schemes, and power conversion devices are explained. Then, the issues related to existed technologies based on past works in the literature are briefly reviewed. Finally, the proposed target of this dissertation is outlined.

1.1 Background

The large penetration of Renewable Energy Resources (RES) has added a large power density to the existed power system. This increased power density and efficiency have brought many challenges to emerged, such as; power quality, power delivery, and transmission, as it is illustrated in Fig. 1.1.

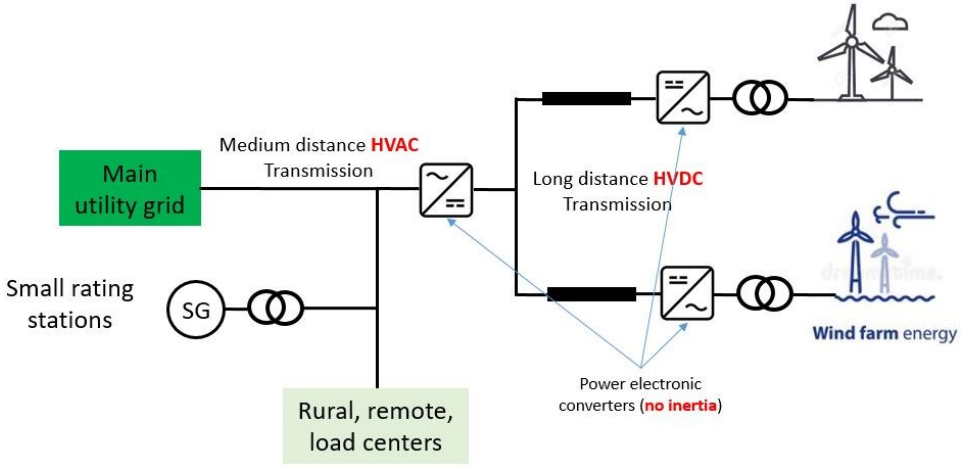

Fig. 1.1 An example of a future power grid configuration.

Numerous topologies and schemes have been suggested to deal with power control and transmission issues. Especially, when now, the expansion in the power systems in the shape of wind farms, which are located far from the load centers, and thus, require a long distance of transmission. For farther wind farms installations, current trends in research and practice point towards the use of High Voltage Direct Current (HVDC) transmission with Voltage Source Converter (VSC) based HVDC transmission being the preferred approach as it displays distinct control and design advantages over traditional Line Commutated Converter (LCC) technology [1]. In such installations, the wind farm collector network typically operates at 50 or 60 Hz, which is then converted to HVDC by a wind farm converter station for transmission to a

load center converter station. VSC-HVDC is currently considered the market leader for wind integration at distances longer than 60-80 km largely due to its established use in point to point bulk power transfer [2].

However, the entire VSC-HVDC existed transmission system has its own limitations starting from the drawbacks of the protection level of the HVDC circuit breakers, to the VSC converter and the existed control approaches used.

1.2 Review of Current Transmission Systems

Conventionally, there are two potential solutions for either power transmission based on the conventional 50 Hz or 60 Hz High Voltage AC.

The HVAC cable transmission system is used for medium distances (up to 80 km), which offers advantages, such as more reliability of the well-known protection schemes and the change capability of voltage levels using transformers [3]. However, the HVAC transmission system's main disadvantage is the existence of reactive power in comparison to no reactive power in the HVDC electrical energy system. Due to that, the existence of the reactive power can be translated as losses in the grid [4]. Moreover, the HVAC system has a low transient stability characteristic.

On the other hand, the HVDC system is broadly applied for point-to-point interconnection of two power systems. Moreover, it is well known for interconnecting the offshore wind farm with the onshore stations using a submarine cable. However, the existence of the power electronic switches in the dc circuit breakers of the HVDC system makes them more vulnerable than the HVAC transmission system, especially when a fault takes place in the converter, due to the low dc-side impedances and sensitive semiconductor power converters. Moreover, the HVDC system current has no zero-crossing points, and thus it will require time in order to disconnect the system [5], [6]. In addition, the existing topologies used with the HVDC system have their own limitations. For example, the line-commutated converter based HVDC (LCC-HVDC) still remains the dominant technology for long-distance bulk power transmission due to lower investment costs and high maximum power transfer capacities. It naturally is able to withstand short circuit currents due to dc inductors limiting the current during fault conditions. Power reversal, however, the multiterminal DC (MTDC) system usually needs a complicated switching technique in the case of using LCCs [7].

In contrast, a VSC-HVDC system is sensitive to faults on the dc lines. When a fault occurs on the dc side of a VSC-HVDC system, the IGBT cannot control and freewheeling diodes work as a bridge rectifier. It is not able to withstand large surge currents and may be damaged before the fault is cleared. Some solutions are proposed, however additional control and switching devices are needed.

Based on the discussion above, the LFAC system is proposed [8] in order to respond to the limitations of both transmission technologies. More details regarding the LFAC system are furtherly discussed in chapter 2.

1.3 Review of LFAC Converters

The ac-ac converter is the core of the power conversion process. The converter acts as an interface between two sides with different frequencies as well as dc transmission. For the LFAC system, many existing applications act as frequency converters choices for the LFAC system. The cycloconverter is one of the most commonly applied choices to connect the LFAC system with the main grid, which is used as a step-down example for several years [9], [10], [11]. Nevertheless, one of the cycloconverter drawbacks is that it is a line-commutated converter, and thus, it is difficult to use in a weak grid. In addition, the cycloconverter has a low power factor and poor quality of output voltage response. They can be represented by the existence of a significant low order harmonic distortion that calls to the need for using large filters [12].

On the other hand, the back-to-back modular multilevel converter (BTB-MMC) in which two MMC type AC/DC converters are connected by a back-to-back scheme is often employed to the HVDC system [13]. However, with the use of the M3C instead of MMC, the number of converters, converter arms can be reduced, and the HVDC links can be eliminated [14]. Moreover, when the BTB-MMC is employed for the LFAC system, current commutation among bridge legs in the MMC is conducted along with the low-frequency system. As a result, the current in the MMC circuit tends to concentrate in the arm for a long time. Therefore, derating of power devices is required for the design of converters.

1.4 Review of Existed Control Schemes

Generally, in terms of power control, existed approaches are dc voltage and active power droop control (V-P) or dc-link voltage versus active power versus frequency control (V-P-ω) for the VSC-HVDC system [15], [16], [17]. These control methods can offer controlled power and interconnection between the main utility grid and/or remote grid using the HVDC system. Moreover, a conventional method of power control using the dq coordination frame with a Phase Locked Loop (PLL) is usually implemented.

Previous work on the M3C control scheme for LFAC system is based on controlling the power on a dq coordinate frame with a Phase-Locked Loop (PLL) for power synchronization. However, this conventional control method has limitations [18], [19], such as:

1- Weak dynamics response.

2- The system configuration cannot be extended.

3- The M3C-LFAC system cannot be operated autonomously, which requires a mean of communication
4- Most importantly, it lacks inertia property and thus it does not enjoy the dynamic features of a Synchronous Generator (SG), which can overcome all the mentioned limitations.

1.5 Research Objectives

From the previous reviews on the existed transmission technologies, ac/ac converters and control schemes, they have shown that the existed HVAC and HVDC transmission systems are becoming more sensitive to grid evolution. The length of the HVAC system and its transient response are not well serving the power grid expansion. The HVDC system can be more applicable than the HVAC system except for its fault tolerance, which is weaker. Thus, in this study, LFAC transmission has been introduced as an alternative. However, the current ac/ac converters are also showing some fatal drawbacks and cannot well contribute to the formation of a reliable and flexible LFAC power grid. From this, the M3C is introduced as a promising converter to create the LFAC power grid. Although the M3C has been successfully employed for the wind energy conversion system, it is based on the conventional controller which has limitation in providing an inertial response, power synchronization and transient blocking.

In order to propose a reliable system, a Virtual Synchronous Generator (VSG) control instead of the conventional control is proposed to the M3C-LFAC system. This combination can open a wide door of various applications that can be applied. This set can resolve all the aforementioned challenges related with the evolution of the power grid.

The main objectives of this study is to construct the LFAC network and confirm its ability to support the existed power grid.

Detailed discussion in the following chapters are organized as follows; at the beginning, in chapter 2 comparison is made between the existed technologies and the proposed ones based on the previous works done in the literature. In the following chapter 3, a point-to-point configuration of M3C-LFAC system is built using a VSG control. Afterwards, the point-to-point configuration is extended to include a multiterminal configuration. Different operating modes based on the speed governor control scheme are applied to add an autonomous operation property to the system. Finally, the M3C-LFAC system using a dual VSG control to interconnect the M3C-LAFC system with a remote ac grid in order to help in frequency regulation and fault ride through, which is investigated in chapter 5.

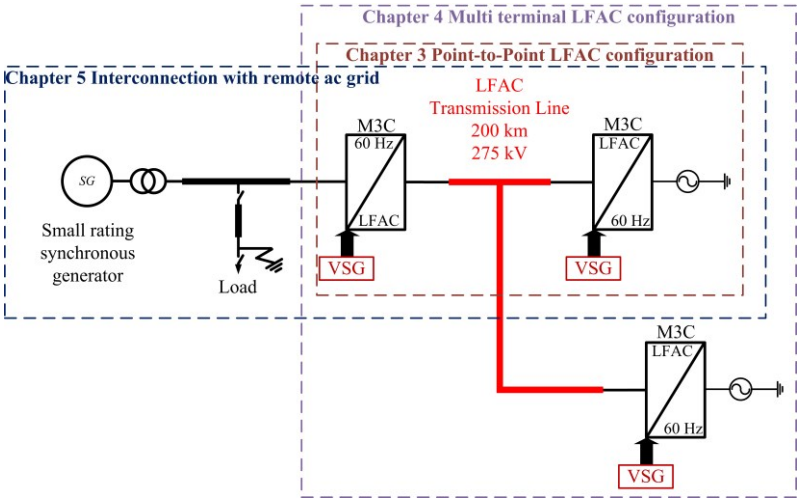

Fig. 1.2 The configuration of the M3C-LFAC system-based VSG control applications of chapters 3, 4, and 5.

1.6 Summary

This chapter started with introducing the major challenges facing the existed power grid due to the increased power density caused by the expansion of the power grid. The feasibility of the available technologies that deal with the expansion of the power grid in terms of amount, distance, and stability is discussed as well as the limitations and the possible solutions provided. With the proposed LFAC transmission system driven by M3C-based VSG control, these issues can be overcome. Moreover, to enable synchronous generator (SG) characteristics to the system, a VSG control is incorporated, which has opened a wide gate of available applications that the M3C-LFAC system can contribute.

References

[1] Madariaga, Ander & Martín, José & Zamora, I. & Martinez de Alegria, Inigo & Ceballos, Salvador. (2013). Technological trends in electric topologies for offshore wind power plants. *Renewable and Sustainable Energy Reviews*. 24. 32 - 44. 10.1016/j.rser.2013.03.039.

[2] Rodrigues, S. & Restrepo, C. & Kontos, Epameinondas (Minos) & Pinto, R. & Bauer, P.. (2015). Trends of offshore wind projects. *Renewable and Sustainable Energy Reviews*. 49. 1114-1135. 10.1016/j.rser.2015.04.092.

[3] Belda, N.A.; Plet, C.A.; Smeets, R.P.P. Analysis of Faults in Multiterminal HVDC Grid for Definition of Test Requirements of HVDC Circuit Breakers. *IEEE Trans. Power Deliv.* 2018, *60*, 403–411.

[4] Chen, J.; Dou, Y.; Li, Y.; Li, J.; Li, G. A Transient Fault Recognition Method for an AC-DC Hybrid Transmission System Based on MMC Information Fusion. *Energies* 2017, *10*, 23.

[5] Bevrani, H.; Watanabe, M.; Mitani, Y. *Power System Monitoring and Control*; IEEE-Wiley press: New York, NY, USA, 2014.

[6] Bozhko, S.V.; Blasco-Giménez, R.; Li, R.; Clare, J.C.; Asher, G.M. Control of offshore DFIG-based wind farm grid with line-commutated HVDC connection. *IEEE Trans. Energy Convers.* 2007, *22*, 71–78.

[7] V. Lescale, A. Kumar, L. E. Juhlin, H. Bjorklund, and K. Nyberg, "Challenges with multi-terminal UHVDC transmissions", *Power System Technology and IEEE Power India Conference*, New Delhi, India, pp. 375-381 (12-15 October, 2008).

[8] X. Wang, X. Wang, "Feasibility study of fractional frequency transmission system", *IEEE Trans. Power Syst*., vol. 11, no. 2, pp. 962-967, May 1996.

[9] Ruddy, J.; Meere, R.; O'Donnell, T. Low Frequency AC transmission as an alternative to VSC-HVDC for grid interconnection of offshore wind. *In Proceedings of the 2015 IEEE Eindhoven Power Tech, Eindhoven*, The Netherlands, 29 June–2 July 2015.

[10] Fischer, W.; Braun, R.; Erlich, I. Low frequency high voltage offshore grid for transmission of renewable power. *In Proceedings of the 3rd IEEE PES Innovative Smart Grid Technologies Europe (ISGT Europe)*, Berlin, Germany, 14–17 October 2012.

[11] Cho, Y.; Cokkinides, C.J.; Meliopoulos, A.P. Time domain simulation of a three-phase cycloconverter for LFAC transmission systems. *In Proceedings of the IEEE PES Transmission and Distribution Conference and Exposition (PES T&D),* Orlando, FL, USA, 7–10 May 2012.

[12] Chen, H.; Johnson, M.H.; Aliprantis, D.C. Low-Frequency AC Transmission for Offshore Wind Power. *IEEE Trans. Power Deliv.* 2013, *28*, 2236–2244.

[13] Nami, A.; Liang, J.; Dijkhuizen, F.; Demetriades, G.D. Modular multilevel converters for HVDC applications: Review on converter cells and functionalities. *IEEE Trans. Power Electron.* 2015, *30*, 18–36.

[14] Wang, K.; Li, Y.; Zheng, Z.; Xu, L. Voltage balancing and fluctuation suppression methods of floating capacitors in a new modular multilevel converter. *IEEE Trans. Ind. Electron.* 2013, *60*, 1943–1954.

[15] T. M. Haileselassie and K. Uhlen, "Impact of DC Line Voltage Drops on Power Flow of MTDC Using Droop Control," in *IEEE Trans. on Power Sys*, vol. 27, no. 3, pp. 1441-1449, Aug. 2012.

[16] R. T. Pinto, S. F. Rodrigues, P. Bauer and J. Pierik, "Comparison of direct voltage control methods of multi-terminal DC (MTDC) networks through modular dynamic models," *Proceedings of the 2011 14th European Conference on Power Electronics and Applications*, Birmingham, 2011, pp. 1-10.

[17]M. Guan, W. Pan, J. Zhang, Q. Hao, J. Cheng and X. Zheng, "Synchronous Generator Emulation Control Strategy for Voltage Source Converter (VSC) Stations," in *IEEE Transactions on Power Systems*, vol. 30, no. 6, pp. 3093-3101, Nov. 2015.

[18]S. Liu, X. Wang, Y. Meng, P. Sun, H. Luo, and B. Wang, “A decoupled control strategy of modular multilevel matrix converter for fractional frequency transmission system,” *IEEE Trans. Power Del.*, vol. 32, no. 4, pp. 2111–2121, Aug. 2017.

[19]Y. Miura, T. Mizutani, M. Ito, and T. Ise, “Modular multilevel matrix converter for low frequency AC transmission,” in *Proc. 2013 IEEE 10th Int. Conf. Power Electron. Drive Syst*., 2013, pp. 1079–1084.

Chapter 2
Review of Related Technologies

2.1 Low Frequency AC Transmission Technology

2.1.1 Overview

LFAC has been utilized for almost a century in railway systems in Germany, Austria, Switzerland and Norway. The traction system in these European countries utilizes 16.7 Hz and some train systems in the USA use 25 Hz [1]. In the early 1900s all traction systems were coal-based, however, prior to the First World War, coal shortages forced train operators to develop electric traction systems. DC drives were the motor of choice for controllable speed, however, DC could not be transformed easily and therefore long-distance railway lines were not a viable option with DC [2]. Universal motors were then used, however when fed AC at standard distribution frequency the large inductance of the windings made the design of large motors impractical. Furthermore, eddy currents induced at standard frequencies caused overheating and reduced efficiency [3]. The solution was to use powerful propulsion motors at a lower frequency to reduce eddy current losses and reduce the complexity of the design. The lower frequency was created using a motor-generator pair. From this, the rail network of 16 Hz was developed (1/3 of 50 Hz) [2], and was altered slightly to 16.7 Hz during the 1990s for stability purposes. The increased use of static power electronic converters made the transition from 16 Hz to 16.7 Hz less difficult. Lower frequency also has the advantage that train tracks can have large distances between electrical sub-stations, which are advantageous for long railway lines.

LFAC was first proposed for high power transmission by Xifan Wang in 1994 [4] in the form of a Fractional Frequency Transmission System (FFTS), which uses lower frequency to reduce the reactance of AC transmission system. The motivation behind the FFTS was to transmit hydro resources from the west of China to the large load centers in the east and south coast. At the time the conventionally used DC transmission was deemed too expensive, and the highest voltage HVAC transmission was 550 kV, which limited the distance [4]. FFTS at a frequency of 50/3 Hz was proposed as a solution to this issue. They concluded that FFTS can increase the amount of transmissible power. For example, their calculations, which were based on examination of the power-angle curves at different frequencies, indicated that for a 550 kV, 1200 km transmission line at 50Hz the transmission power limit was 850 MW, whereas with FFTS the limit was 1700 MW. In a follow-up paper, the same group demonstrated a scaled hardware model of the frequency-changing converter [5]. A scaled model was produced from a hydro plant, with

the generator configured to produce 16.7 Hz (adding extra poles to the generator), connection via LFAC transmission to the load center 1200 km away, and connecting to the local grid via a frequency changer, in this case, a cycloconverter. The analysis concluded that LFAC could reduce the number of lines required, by increasing the maximum power transfer capability of AC cables. It was also concluded that the cycloconverter could change the frequency from 16.7 to 50 Hz; however, there were concerns with the low power factor and the introduction of significant harmonics in the output voltage from the thyristor switching. The feasibility of connecting large-scale wind generation at a long distance from the load center is further investigated in Wang et al. [6], via FFTS or LFAC. Again, the motivation was to reduce the investment cost required for transmission of vast wind resources 915 km from the biggest load centers. The authors present a specific case study comparing conventional 50 Hz transmission and FFTS to integrate 10,000 MW of wind power. A power flow analysis concludes that the voltage variation of the 50 Hz system spends more time outside the voltage limit of 5% than the variation at FFTS. Therefore, the FFTS system can transmit more wind power without curtailment due to voltage constraints. It is interesting to note that an HVDC option is not included in this analysis as this could be the most feasible way of transmitting power at such distances. The authors concluded that the added cost of larger transformers and the frequency changer may make the system more expensive. Further work considering the power flow in an FFTS system connected to onshore wind farms is presented in [7]. The steady-state performance of LFAC with transmission lines and a cyclonconverter as the frequency-changing converter is presented in [8]. A range of operating frequencies is examined from 5 to 60 Hz with the conclusion that the lower frequency systems have a superior voltage profile due to the reduced voltage drop, adding to the potential benefits of LFAC for bulk power transmission. It has also been proposed that LFAC may be used to interconnect two grids, which operate at different frequencies or voltages, in much the same way as HVDC has done in many cases [9]. Funaki and Matsuura [4] propose LFAC transmission and compare it to both HVAC and HVDC transmission in the form of a feasibility study for interconnecting two grids. The basic operation was demonstrated and confirmed by transient simulation. A control system was implemented based on the swing equation to maintain frequency stability in the simulation. Simulation results indicated that the LFAC system had comparable control compared to an HVDC system in terms of AC power flow control; however, the low order harmonics on the output of the frequency converter are a concern.

2.1.2 Comparison with Existing Transmission Technologies

HVAC cables have two main limiting factors, which limit the power transfer capability of the cable. These are the maximum allowable voltage deviation at the receiving end of the cable, and the cable current carrying capability. Current carrying capability is a combination of the active current and the charging current (reactive current) which depends on the frequency, length and capacitance of the cable [10]. As

can be seen from Equation 2.1, at lower frequencies the charging current is reduced, therefore reactive power generated in the cable is reduced, from Equation 2.2, leaving more space for active power, thus increasing the current carrying capability, and the maximum active power calculated by Equation 2.3.

$$I_C = 2\pi f l C E \tag{2.1}$$

$$Q_C = I_C E \tag{2.2}$$

$$P_R = \sqrt{S^2 - Q_C^2} \tag{2.3}$$

where E rated voltage, f frequency, l length of cable, C cable capacitance per unit length, S apparent power, P_R maximum active power transmission capability.

To increase the transmission capability of a cable, the options are to increase the voltage or decrease the inductive reactance of the cable. If a cable is operated at a lower frequency, its inductive reactance decreases resulting in a reduced voltage deviation across the cable reduced charging current and therefore reduced generated reactive power. This results in an increase in active power that can be transmitted in the cable P_R.

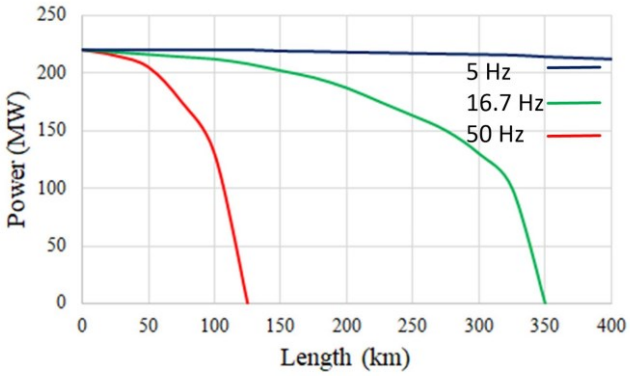

Fig. 2.1: Transmission capability curves for 220 kV, 1000A cable at different frequencies.

Fig. 2.1 shows the effect of alternative frequencies on a 220 kV 3 core XPLE subsea transmission cable. It can be seen in Fig. 2.1 that a reduction in frequency provides an increased maximum length that power can be transmitted through an offshore cable. The maximum distance allowed is limited by the voltage deviation constraint at the receiving end. For transmission, at 16.7 Hz the maximum distance allowable is almost three times that at 50 Hz [4].

On the other hand, the HVDC system is well preferred for long-distance transmission and for submarine transmission cables especially to connect offshore wind farms with an onshore grid. However, with the HVDC system technology, a few major technical challenges need to be addressed before such systems, with dc side protection, are realized. One of the main challenges is the lack of fast, low loss and reliable

HVDC circuit breakers (CBs) capable of clearing dc faults. Therefore, an intensive investigation (which is being done) for improving the HVDC Circuit Breakers (CBs) is required in order to improve its fault tolerance as well as response.

2.2 Modular Multilevel Matrix Converter

2.2.1 Introduction

The Multilevel Matrix Converter (Multilevel MC) is a basic type of the direct ac/ac multilevel converter family which was created for applications which required a good harmonic and conversion factors and to solve the problem of low converter efficiency at low voltage, low power [11], [12]. A schematic of the converter with a basic configuration is illustrated in Fig. 2.2(a). The converter is a hybrid of multilevel and matrix technologies. The conversion approach of the converter is based on H-bridge switch cell. The use of a matrix configuration eliminates the need for DC voltage sources to supply average power. Therefore, the DC voltage sources can be replaced by DC capacitors, as shown in Fig. 2.2(b). The Multilevel MC synthesizes the input and the output voltages by space vector pulse width modulation (SVPWM) of the DC capacitor voltages of the H-bridge switch cells. This operation differs from that of the conventional matrix converter in which the voltages are synthesized on one side and currents on the other. Therefore, inductors can be used as filter elements on both sides of the converter. Because of the symmetry of the multilevel matrix converter structure, both step-up and step-down of the voltage magnitude are possible.

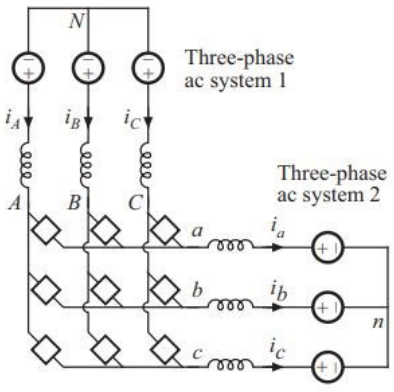

(a)

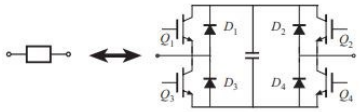

(b)

Fig. 2.2 Basic configuration of a multilevel matrix converter: (a) converter topology, (b) schematic of an H-bridge switch cell

Similarly, for same applications mentioned for the multilevel MC but aiming at high voltage and high power ratings, a Modular Multilevel Matrix Converter (M3C) was created. The M3C has advantages over traditional topologies including modularity, a simple extensions to enable operation at high voltage levels with options for redundancy, control flexibility and enhanced waveform quality [13], [14]. The basic structure of the M3C is shown in Fig. 2.3, which is almost similar to the relevant Modular MC except that the arms of the converter are constructed of number of H-Bridge switch cells, the increased number of the cells is decided in order to enable the converter to be suitable to operate in high ratings conditions.

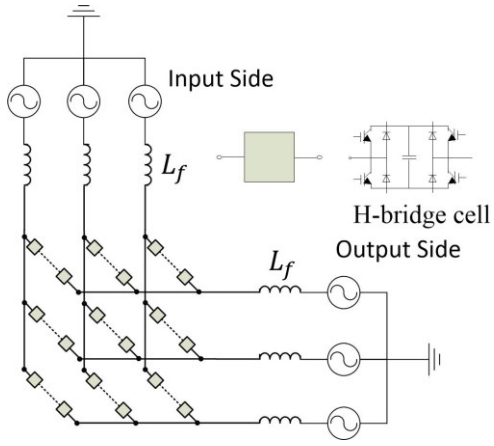

Fig. 2.3 Basic structure of a modular multilevel matrix converter (M3C).

2.2.2 Applications

Using an M3C for the integration of LFAC offshore wind power was proposed by Miura et al. [15] and an updated control strategy for M3C in LFAC systems has been presented in [16]. In [15] it is shown that in theory, the multilevel matrix converter can act as the onshore frequency changer, with active and reactive power control [17].

Another application that uses the M3C is in a mill drive to work as a low-speed, high-torque motor drive application that was proposed by Kawamura et al. [18]. This work provided experimental verification of a modular multilevel cascade converter based on triple-star bridge cells (MMCC-TSBC). A downscaled motor drive, combining a 400-V, 15-kW TSBC equipped with four bridge cells per cluster and a 320-V, 38-Hz, 6-pole, 15-kW induction motor loaded at the rated torque has been designed, constructed and tested to verify the effectiveness and viability of the motor drive. The authors of this work found out that the M3C is suitable for such applications due to the absence of circulating currents. This comes from the

principle configuration that requires to connect an inductor with each converter arm and thus, it allows the M3C to control four independent circulating currents for dc-voltage balancing and ac-voltage mitigating of all the floating dc capacitors [19].

2.2.3. Existed Control Methods

The conventional control scheme for the M3C consists of two parts that must be performed simultaneously: (1) terminal AC voltage synthesizing and (2) capacitor voltage regulating. The space vector pulse width modulation (SVPWM) technique is employed for synthesizing the terminal AC voltages. The single-capacitor control scheme and the capacitor voltage-balancing scheme, which are based on the space vector modulation (SVM), are proposed for the multilevel matrix converter operating in the two-level switching mode. The SVM is performed in the dq coordinate; hence, the three-phase variables are transformed into two-phase dq variables. The M3C converter can generate several combinations of the three-phase line-line voltages corresponding to multiple space vectors in the dq coordinate.

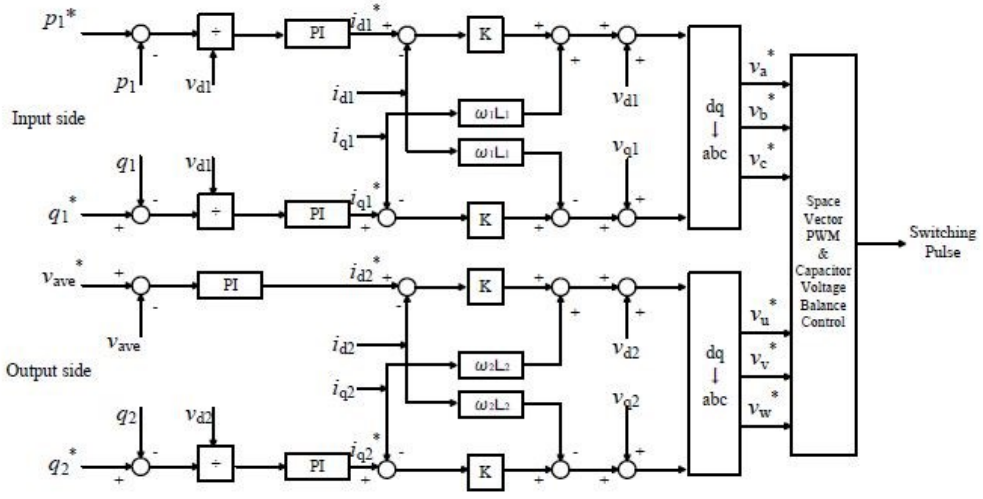

Fig. 2.4 Configuration of control system of M3C

The conventional control of the M3C starts with power control and capacitor average voltage control. Fig 2.4 shows the configuration of the conventional control system of M3C. This control consists of two parts; the input side part and output side part, in which both are controlled in dq coordination frame. The dq transformation is a method of converting three-phase alternating current from a three-phase stationary coordinate system to a two-phase rotating coordinate system, and it is carried out by equation (2.4). Here,

ω represents angular frequency, which is obtained from the Phase-Locked Loop (PLL). When the dq conversion is performed, the measured voltages and currents are converted to direct current. For this reason, the control on the dq coordinate system can make the steady-state deviation of the voltages and currents zero, unlike the control on the stationary coordinate.

$$[C] = \sqrt{\frac{2}{3}}\begin{bmatrix} cos(\omega t) & cos\left(\omega t - \frac{2\pi}{3}\right) & \cos\left(\omega t - \frac{4\pi}{3}\right) \\ -sin(\omega t) & -sin\left(\omega t - \frac{2\pi}{3}\right) & -sin\left(\omega t - \frac{4\pi}{3}\right) \end{bmatrix} \tag{2.4}$$

Each part of the conventional control combines outer power control and inner current control. The outer part control task is to control active and reactive power and to generate the reference currents. On the other hand, the inner control generates the reference dq coordinate voltages to be used later in the SVPWM for determining the switching pulses. Generally, in order to keep the capacitor average voltage constant in steady-state, instead of controlling the active power on the output side, a capacitor average voltage control is required instead. The active power is expressed by equation (2.5) on the dq coordinate.

$$p = v_d i_d + v_q i_q \tag{2.5}$$

Also, when dq conversion is performed with the d-axis of the system voltage as a reference, from v_q = 0,

$$p = v_d i_d \tag{2.6}$$

On the dq coordinate, the reactive power is expressed by equation (2.7)

$$q = v_d - v_q i_d \tag{2.7}$$

Also, when dq conversion is performed with the d-axis of the system voltage as a reference, from v_q = 0,

$$q = v_d i_q \tag{2.8}$$

M3C outputs a voltage with the capacitor in the cell as a DC voltage source and controls the AC current. When the capacitor voltage in all the cells is greatly reduced, it becomes impossible to output the voltage required for controlling the AC current, which is determined by the rated voltage of the system. On the other hand, when the capacitor voltage in all the cells is greatly increased, the number of cells for outputting the voltage necessary for the AC current control becomes small. In this case, the number of levels of the output voltage decreases and the harmonic wave increases. Besides, overcharging of the capacitor also leads to failure. Therefore, it is desirable that the average value of all capacitors is a constant value.

However, when the sum of the active power p_1 on the input side, the active power on the output side p_2, and the circuit loss P_{loss} is not 0, the voltage of all the capacitors is decreased or increased, and the voltage of all the capacitors fluctuates. Therefore, in order to keep the total capacitor voltage of the M3C at a constant value, active power control is performed on the input side, and feedback control is performed on the output side by using the average value V_{ave} of the capacitor voltage as shown in Fig. 2.4, and is calculated based on the average sum of all H-bridge cells capacitors voltages as

$$V_{ave} = \sum_{\substack{x=a,b,c \\ y=u,v,w \\ i=1,2,\ldots,n}} \frac{v_{xyi}}{9n} \tag{2.9}$$

where, i represents the number of the cell's measured voltage.

The control principle of the average value of the voltage, that is, when the average value of the capacitor voltage is higher than the command value, the active power on the output side is controlled so that all the capacitors are discharged. Whereas, when the average value is lower than the command value, the active power on the output side is controlled to charge. By this control, the average value of the total capacitor voltages is controlled to a constant value.

To determine PWM pattern from the voltage references, a voltage space vector scheme is used. The capacitor in each H-bridge cell is regarded as a voltage source and various line-to-line voltages can be realized by a combination of the output voltage of these cells. Available line-to-line voltage vectors of the 7-level M3C are shown in Fig. 2.5. Each vertex represents a terminal point of each voltage vector. A voltage reference vector (V_{ref}) is realized by a combination of three voltage vectors whose terminal points configure the triangle containing the terminal point of the voltage reference vector (V_{k_in}, V_{l_in}, V_{m_in}) for input side power system which are calculated using (2.10) and (2.11) for systems #1 and #2.

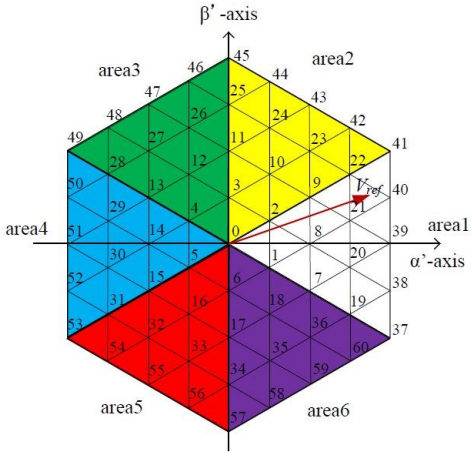

Fig. 2.5 Voltage vector diagram between the output lines of the 4-stage M3C

$$V_{ref} = d_{k\_in}V_{k\_in} + d_{l\_in}V_{l\_in} + d_{m\_in}V_{m\_in} \tag{2.10}$$

$$d_{k\_in} + d_{l\_in} + d_{m\_in} = 1 \tag{2.11}$$

Duty ratios (d_{k_in}, d_{l_in}, d_{m_in}) for the input side power system are also calculated using voltage vectors (V_{k_in}, V_{l_in}, V_{m_in}) in the same way. Finally, each voltage vector is output in one sampling period (Ts) according to the timing chart shown in Fig. 2.6. Similar determination for the duty ratios and voltage vectors is done in the output side power system.

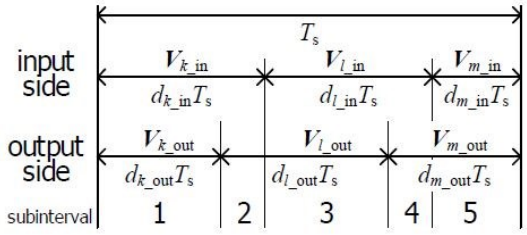

Fig. 2.6. Timing chart for input voltage vectors.

2.3 Virtual Synchronous Generator Control

2.3.1 Introduction

In this section, the virtual synchronous generator (VSG) concept was introduced as a promising solution towards the grid stability issues caused by high penetration RES in the electrical grid. A VSG can be established by using short-term energy storage systems coupled with the power electronics inverter/converter with the proper control mechanism [20]. In addition, since it depends on the existence of the energy storage system (such as capacitors), it can be expected to implement the VSG for the M3C control.

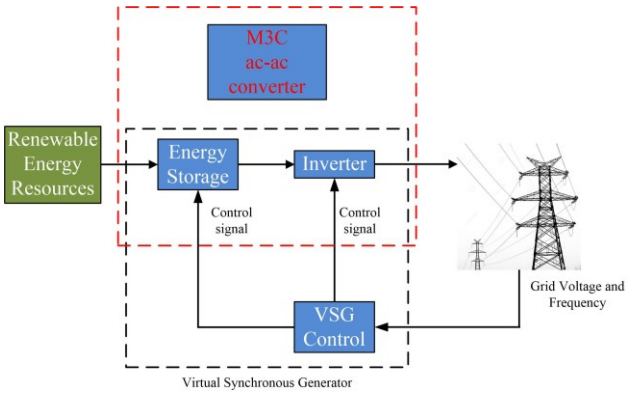

Fig. 2.7 General structure of VSG and adaptation for M3C

The general architecture of VSG is presented in Fig. 2.7. In this scheme, a distributed generator (DG)/RESs unit is connected to the grid via VSG. It is expected to operate as a conventional synchronous generator by providing inertia and damping property virtually and by displaying the same reaction as the conventional synchronous generator when there is a sudden change of load or disturbance in the system. The VSG control block is expected to regulate the output of the inverter based on the rate of change of frequency and the difference between the reference frequency and grid frequency much like the way conventional synchronous generators are governed by the swing equation:

$$\Delta P_{VSG} = P_m - P_e = J\Delta\omega + D\Delta\omega \tag{2.12}$$

where *J* is the inertia coefficient and *D* is the damping coefficient. *Pm*, *Pe*, and $\Delta\omega$ are; input mechanical power, output electrical power and frequency deviation, respectively.

In contrast, for a robust transient stability, it is essential for any power system to include a swing equation as it represents the heart of a power system. The swing equation describes the relative motion of the rotor with respect to the stator field as a function of time and is given by [21], [22]

$$\tau_m(t) - \tau_e(t) = J\frac{d^2}{dt^2}\delta(t) + D\frac{d}{dt}\delta(t) \tag{2.13}$$

where $\boldsymbol{\tau_m}$ is the rotor electromagnetic torque, $\boldsymbol{\tau_e}$ is the mechanical torque, $\boldsymbol{\delta}$ is the rotor angular position difference from its reference position, $\boldsymbol{t}$ is the time in second. The generator inertia reacts to the disturbance and plays a significant role in power system stability, which is the most important property of a synchronous machine.

2.3.2 Conventional Virtual Synchronous Generator Control

The concept of VSG was introduced in 2007 as a method of resolving stability problems in the power grid due to the integration of renewable energy sources [23], [24]. Many research groups are still working to develop various designs and control strategies to replicate the inertia and damping properties of conventional synchronous generators. The concept of Synchroconverter was also introduced [25] that mimic properties of synchronous generators. The most active research groups working on VSG's are; VSYNC project under the 6th European Research Framework program [23], [26], [30], the Virtual Synchronous Machine (VISMA) project [31], [34] at the Institute of Electrical Power Engineering, (IEPE) at the Clausthal University of Technology in Germany, the VSG research team at Kawasaki Heavy Industries (KHI) [28], and the ISE Laboratory in Osaka University [20], [35], [37] in Japan. In this subsection, the latest VSG is described, which is developed to control the M3C-LFAC system in this work.

The VSG developed by Ise's lab at Osaka university is meant for inverter-based distributed generators (DGs), cycloconverter in LFAC system, and HVDC transmission, and it has further been developed to operate with the M3C-based LFAC transmission systems environment shown in Fig 2.8.

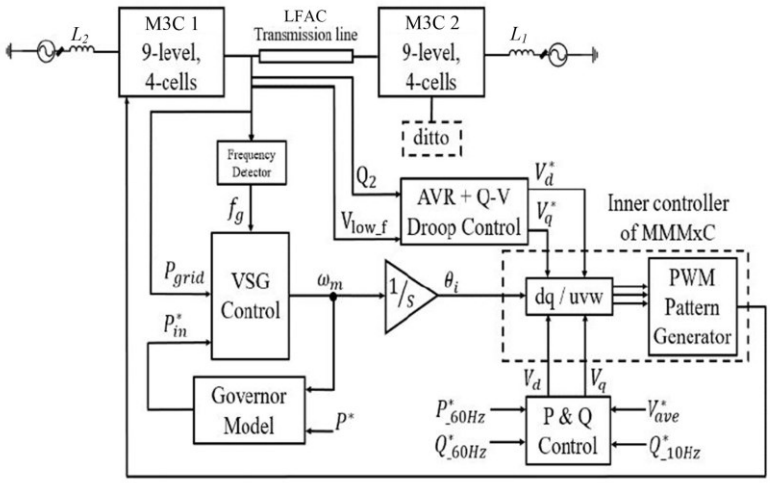

Fig. 2.8 VSG Structure developed for M3C-LFAC system

In this model, the swing equation used by Ise's lab is adapted to work in synchronism along with the conventional control to operate the M3C. The swing equation for this model can be expressed by the following equation

$$P_{in} - P_{out} = J\Delta\omega_m \frac{d\Delta\omega_m}{dt} - D\Delta\omega_m \tag{2.14}$$

where P_{in} is the input power, i.e., prime mover power to a synchronous machine, P_{out} is the output power of the VSG, and ω_m is the rotor speed. This swing equation plays a vital role in this VSG model. Based on the relation between the VSG input and output power (as explained in equation (2.14)), they set the reference real power P_{in}. Output power P_{out} and the grid frequency are measured by the power/frequency meter. Using the swing equation, the VSG controller provides the virtual rotational speed ω_m. Numerical integration of this rotational speed ω_m as in equation (2.14), will deliver the virtual mechanical phase angle θ_m to PWM for generating pulses.

The M3C generally, requires two independent controls on both input and output sides. Due to this freedom and depending on the applications, it is used for any control scheme, which can be implemented. For example, based on Fig. 2.8, a VSG control is included for the LFAC side while a conventional control is controlling the grid side. If a certain application requires frequency support, from the frequency stability

point of view, it is more reliable to replace the conventional control with another VSG control, thus the M3C will have two VSGs control schemes on both sides.

2.3.3 Applications of Virtual Synchronous Generator Control

The objective of the VSG scheme is to reproduce the dynamic properties of a real synchronous generator (SG) for the power electronics-based units, in order to inherit the advantages of an SG in stability enhancement. The application of VSGs in power systems has been reported in the research [38], [41]. For example, an improved VSG controller was proposed in [38] by linearizing and decoupling voltage deviation and damping factor in order to suppress output power oscillations. In [39], VSG was used to propose an adaptive active power and dc voltage droop control for multi-terminal HVDC (MTDC) systems. As another example, [40] provided a comparison of simple frequency droop control and VSG control using small-signal models. The VSG concept was successfully implemented in [42] for multi-terminal HVDC systems in order to propose a systematic control method that:

1) Resolves the problem of low-frequency oscillation.
2) Enhances the power oscillation damping performance of the ac/dc system.

In fact, VSG provides numerous advantages to the power system stability in various applications.

2.4. Summary

This chapter provides a review of the related technologies introduced in this dissertation. Starting from the Low-Frequency AC (LFAC) transmission, which is of significant interest for power transmission as an adaptation of HVAC transmission. The key advantage of the LFAC system compared to the HVDC system is the reliable dependence on the use of the circuit breakers inherited from the conventional HVAC as well as reduced losses and extended transmission distance compared with the conventional HVAC. A comprehensive review of existing research conducted on LFAC and a discussion centering on the design considerations for LFAC transmission is presented.

The M3C is explained in details as a promising technology to handle the LFAC system for high ratings. The M3C conventional controller is discussed as state-of-the-art for the M3C control in addition to the space vector pulse width modulation (SVPWM) technique used inside the M3C control.

Finally, the VSG control is introduced and discussed as a key solution to adapt the M3C-LFAC for promising applications. The brief history about the VSG control is discussed and the contribution towards the development of this control scheme by several teams is presented in addition to introducing the conventional VSG which is used in this work.

References

[1] A. Pfeiffer, W. Scheidl, M. Eitzmann and E. Larsen, "Modern rotary converters for railway applications," *Proceedings of the 1997 IEEE/ASME Joint Railroad Conference*, Boston, MA, USA, 1997, pp. 29-33.

[2] K. Weiland, "New technological challenges operating the 110 kV, 16.7 Hz grid for railway power supply in Germany," *CIRED 2009 - 20th International Conference and Exhibition on Electricity Distribution - Part 1*, Prague, Czech Republic, 2009, pp. 1-3.

[3] S. Frey, Railway Electrification Systems & Engineering. White Word Publications, 2012.

[4] T. Funaki and K. Matsuura, "Feasibility of the low frequency AC transmission," *2000 IEEE Power Engineering Society Winter Meeting. Conference Proceedings (Cat. No.00CH37077)*, Singapore, 2000, pp. 2693-2698 vol.4, doi: 10.1109/PESW.2000.847308.

[5] Wang Xifan, Cao Chengjun and Zhou Zhichao, "Experiment on fractional frequency transmission system," in *IEEE Transactions on Power Systems*, vol. 21, no. 1, pp. 372-377, Feb. 2006.

[6] X. Wang, Y. Teng, L. Ning, Y. Meng, and Z. Xu, "Feasibility of integrating large wind farm via fractional frequency transmission system a case study", *International Transactions on Electrical Energy Systems*, vol. 24, no. January 2013, pp. 64-74, 2014.

[7] T. Yufei, W. Xifan, N. Lianhui, M. Yongqing, and S. Zhuoyan, "Unified iterative method to calculate power flow of the interconnected system with Fractional Frequency Transmission System," in *4th International Conference on Electric Utility Deregulation and Restructuring and Power Technologies (DRPT)*, 2011, pp. 438-443.

[8] T. Ngo, M. Lwin and S. Santoso, "Steady-State Analysis and Performance of Low Frequency AC Transmission Lines," in *IEEE Transactions on Power Systems*, vol. 31, no. 5, pp. 3873-3880, Sept. 2016.

[9] Hualei Wang and M. A. Redfern, "The advantages and disadvantages of using HVDC to interconnect AC networks," *45th International Universities Power Engineering Conference UPEC2010*, Cardiff, Wales, 2010, pp. 1-5.

[10] J. Song-Manguelle, M. Harfman Todorovic, S. Chi, S. K. Gunturi and R. Datta, "Power Transfer Capability of HVAC Cables for Subsea Transmission and Distribution Systems," in *IEEE Transactions on Industry Applications*, vol. 50, no. 4, pp. 2382-2391, July-Aug. 2014.

[11] Al-Naseem, O. A., Modeling and Space Vector Control of a Novel Multilevel Matrix Converter for Variable-Speed Wind power Generators. PhD thesis, University of Colorado, Apr. 2001.

[12]R. W. Erickson and O. A. Al-Naseem, "A new family of matrix converters," *IECON'01. 27th Annual Conference of the IEEE Industrial Electronics Society (Cat. No.37243)*, Denver, CO, USA, 2001, pp. 1515-1520 vol.2.

[13]Erickson, R., Angkititrakul, S., Almazeedi, K.: 'A new family of multilevel matrix converters for wind power applications: final report'. Tech. Rep., University of Colorado, December, 2006.

[14]Okazaki, Y., Kawamura, W., Hagiwara, M., et al.: 'Which is more suitable for MMCC-based medium-voltage motor drives, a DSCC inverter or a TSBC converter?'. 9th Int. Conf. on Power Electronics ECCE Asia: 'Green World with Power Electronics', Seoul, South Korea, June 2015, pp. 1053–1060.

[15]Y. Miura, T. Mizutani, M. Ito and T. Ise, "Modular multilevel matrix converter for low frequency AC transmission," *2013 IEEE 10th International Conference on Power Electronics and Drive Systems (PEDS)*, Kitakyushu, 2013, pp. 1079-1084.

[16]J. Ma, M. Dahidah, V. Pickert and J. Yu, "Modular multilevel matrix converter for offshore low frequency AC transmission system," *2017 IEEE 26th International Symposium on Industrial Electronics (ISIE)*, Edinburgh, 2017, pp. 768-774.

[17]A. Garcés and M. Molinas, "A Study of Efficiency in a Reduced Matrix Converter for Offshore Wind Farms," in *IEEE Transactions on Industrial Electronics*, vol. 59, no. 1, pp. 184-193, Jan. 2012.

[18]W. Kawamura, K. Chen, M. Hagiwara and H. Akagi, "A Low-Speed, High-Torque Motor Drive Using a Modular Multilevel Cascade Converter Based on Triple-Star Bridge Cells (MMCC-TSBC)," in *IEEE Transactions on Industry Applications*, vol. 51, no. 5, pp. 3965-3974, Sept.-Oct. 2015.

[19]W. Kawamura, M. Hagiwara and H. Akagi, "Control and Experiment of a Modular Multilevel Cascade Converter Based on Triple-Star Bridge Cells," in *IEEE Transactions on Industry Applications*, vol. 50, no. 5, pp. 3536-3548, Sept.-Oct. 2014.

[20]K. Sakimoto, Y. Miura and T. Ise, "Stabilization of a power system with a distributed generator by a Virtual Synchronous Generator function," *8th International Conference on Power Electronics - ECCE Asia*, Jeju, 2011, pp. 1498-1505.

[21]Bevrani, H.; Watanabe, M.; Mitani, Y. *Power System Monitoring and Control*; IEEE-Wiley press: New York, NY, USA, 2014.

[22]Bevrani, H. *Robust Power System Frequency Control*, 2nd ed.; Springer: Berlin/Heidelberg, Germany, 2014.

[23]J. Driesen and K. Visscher, "Virtual synchronous generators," *2008 IEEE Power and Energy Society General Meeting - Conversion and Delivery of Electrical Energy in the 21st Century*, Pittsburgh, PA, 2008, pp. 1-3.

[24]T. Loix, S. De Breucker, P. Vanassche, J. Van den Keybus, J. Driesen and K. Visscher, "Layout and performance of the power electronic converter platform for the VSYNC project," *2009 IEEE Bucharest PowerTech*, Bucharest, 2009, pp. 1-8.

[25]Q. Zhong and G. Weiss, "Synchronverters: Inverters That Mimic Synchronous Generators," in *IEEE Transactions on Industrial Electronics*, vol. 58, no. 4, pp. 1259-1267, April 2011.

[26]K. Visscher and S. W. H. De Haan, "Virtual synchronous machines (VSG's) for frequency stabilization in future grids with a significant share of decentralized generation," *CIRED Seminar 2008: Smart Grids for Distribution*, Frankfurt, 2008, pp. 1-4.

[27]V. Karapanos, S. W. H. de Haan, K. H. Zwetsloot, "Testing a virtual synchronous generator in a real-time simulated power system," *Int. Conf. on Power Systems Transients (IPST2011)*, Delft, Netherland, June 2011.

[28]M. Albu, A. Nechifor and D. Creanga, "Smart storage for active distribution networks estimation and measurement solutions," *2010 IEEE Instrumentation & Measurement Technology Conference Proceedings*, Austin, TX, 2010, pp. 1486-1491.

[29]T. V. Van et al., "Virtual synchronous generator: An element of future grids," 2010 *IEEE PES Innovative Smart Grid Technologies Conference Europe (ISGT Europe)*, Gutenberg, 2010, pp. 1-7.

[30]Y. Chen, R. Hesse, D. Turschner, and H. P. Beck, "Comparison of methods for implementing virtual synchronous machine on inverters," *Int. Conf. on Renewable Energies and power quality-ICREPQ*'12, Spain, March 2012.

[31]Y. Chen, R. Hesse, D. Turschner and H. Beck, "Improving the grid power quality using virtual synchronous machines," *2011 International Conference on Power Engineering, Energy and Electrical Drives*, Malaga, 2011, pp. 1-6.

[32]Y. Chen, R. Hesse, D. Turschner, and H. P. Beck, "Dynamic properties of the virtual synchronous machine (VISMA)," *Int. Conf. on Renewable Energies and Power Quality (ICREPQ´11)*, Las Palmas de Gran Canaria, Spanien, April 2011.

[33]R. Hesse, D. Turschner, and H.-P. Beck, "Microgrid stabilization using the virtual synchronous machine," *in Proc. International Conf. on Renewable Energies and Power Quality (ICREPQ'09)*, Spain, 2009.

[34]J. Alipoor, Y. Miura and T. Ise, "Power System Stabilization Using Virtual Synchronous Generator With Alternating Moment of Inertia," in *IEEE Journal of Emerging and Selected Topics in Power Electronics*, vol. 3, no. 2, pp. 451-458, June 2015.

[35]T. Shintai, Y. Miura and T. Ise, "Reactive power control for load sharing with virtual synchronous generator control," *Proceedings of The 7th International Power Electronics and Motion Control Conference*, Harbin, 2012, pp. 846-853.

[36]J. Alipoor, Y. Miura, T. Ise, “Evaluation of virtual synchronous generator (VSG) operation under different voltage sag conditions,” *in Proc. IEE Japan Joint Technical Meeting on Power Engineering and Power Systems Engineering*, Tokyo, Japan, 2012, no. PE-12-60 PSE-12-76, pp. 41-46.

[37]R. H. Lasseter and P. Piagi, “Control and design of micro grid components” Madison, WI, PSERC project rep. no. PSERC-06–03, Jan. 2006.

[38]T. Shintai, Y. Miura and T. Ise, "Oscillation Damping of a Distributed Generator Using a Virtual Synchronous Generator," in *IEEE Transactions on Power Delivery*, vol. 29, no. 2, pp. 668-676, April 2014.

[39]R. Wang, L. Chen, T. Zheng and S. Mei, "VSG-based adaptive droop control for frequency and active power regulation in the MTDC system," in *CSEE Journal of Power and Energy Systems*, vol. 3, no. 3, pp. 260-268, Sept. 2017.

[40]J. Liu, Y. Miura and T. Ise, "Comparison of Dynamic Characteristics Between Virtual Synchronous Generator and Droop Control in Inverter-Based Distributed Generators," in *IEEE Transactions on Power Electronics*, vol. 31, no. 5, pp. 3600-3611, May 2016.

[41]M. Guan, W. Pan, J. Zhang, Q. Hao, J. Cheng and X. Zheng, "Synchronous Generator Emulation Control Strategy for Voltage Source Converter (VSC) Stations," in *IEEE Transactions on Power Systems*, vol. 30, no. 6, pp. 3093-3101, Nov. 2015.

[42]Y. Cao et al., "A Virtual Synchronous Generator Control Strategy for VSC-MTDC Systems," in *IEEE Transactions on Energy Conversion*, vol. 33, no. 2, pp. 750-761, June 2018.

Chapter 3

Point-to-Point Low Frequency AC Transmission System Operation using Modular Multilevel Matrix Converter with Virtual Synchronous Generator Control

3.1 Introduction

The discussion in the previous chapters have theoretically demonstrated that the proposed LFAC, M3C and VSG can individually respond to provide robust features compared with each one's counterpart. Thus, in this chapter, the application of M3C-LFAC system using VSG control for point-to-point configuration is studied. The merits of this system are:

1- The LFAC system is advantageous with a higher power capacity than the commercial frequency high voltage ac (HVAC) system and better fault protection than the high voltage dc (HVDC) system.

2- The M3C enjoys technical features such as; low harmonic content and high power factor than a cycloconverter that is frequently used in the LFAC system

3- The virtual synchronous generator (VSG) is a control strategy that has been proposed to mitigate stability issues in power systems, enabling solid-state converters to imitate synchronous generators' characteristics and can potentially contribute to the future formation of the LFAC expanded network. Moreover, by using the VSG control, the active power can be sent and received automatically and autonomously, thus avoiding the use of the master-slave power control scheme.

3.2 System Configuration

The configuration of the two-terminal model is shown in Fig. 3.1. It is combined of two terminals and each of which has an M3C connected via 275 kV and 200 km LFAC transmission system.

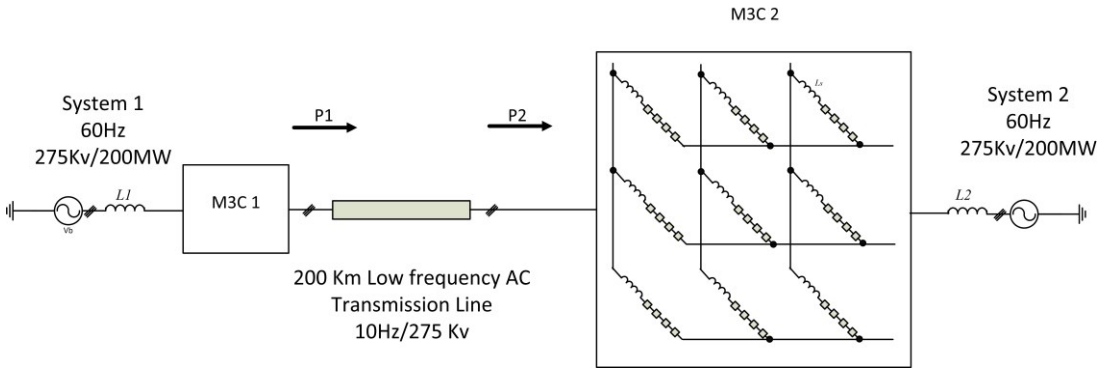

Fig. 3.1 A configuration of two-terminal LFAC system using M3C with VSG control.

Fig 3.2 shows the circuit configuration of the M3C. It consists of nine arms, each arm has four H-bridge cells connected in series, and these cells connect the input side (60 Hz side) to the output side (10 Hz side). Generally, in a large system, each arm will consist of hundreds of H-bridge cells considering the high voltage level, thus the filter inductance L_f can be quite small. However, in this study, the number of cells is reduced to four for simplicity and less computational time of the simulation and a relatively large L_f is used. Small inductors called arm inductors, which are omitted in Fig 3.2, were connected with each converter arm in order to suppress the current flowing at the timing of commutation between those arms.

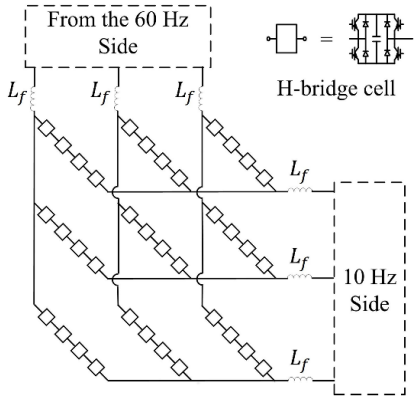

Fig. 3.2 A circuit configuration of a 9-level modular multilevel matrix converter.

The main feature of the M3C is the cascaded connection of a number of power cells that are composed of power electronic devices and the dc capacitor works as a dc voltage source. These cells work as bidirectional switches and can easily be applied for low frequency, high voltage and high-power applications.

It is noteworthy to mention that, there is a tradeoff when selecting the operating frequency of the LFAC system [1], [2]. For instance, if the 20 Hz frequency is selected, it will require to use a smaller transformer

in terms of weight and size as well as for the sub-module capacitor of the M3C [3], unlike the case of 10 Hz, which requires a larger footprint. In contrast, for the 20 Hz frequency, the transmission distance will be reduced compared with the case of 10 Hz. Moreover, the capacitive current for the 20 Hz is larger, as reported in [2], [3]. Therefore, in this work, the 10 Hz frequency is selected merely to operate the MT-LFAC system. The investigation on the optimal frequency of LFAC system is beyond the scope of this dissertation.

3.3 Control Scheme

This section describes the control method of M3C. The overall control scheme of both input (60 Hz) and output (10 Hz) sides is shown in Fig. 3.3.

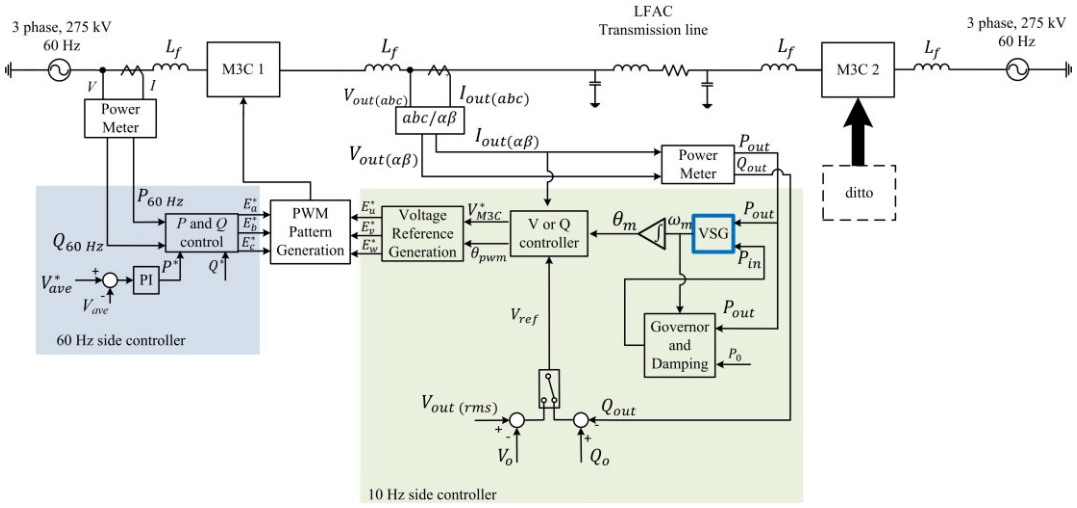

Fig. 3.3. Overall control block diagram of VSG and conventional control

3.3.1 Control Scheme of Converter Current and Capacitor Voltage

According to Fig. 3.3, the control scheme is divided into two parts; the input side (60 Hz side) conventional control part based on dq coordination frame, and the output side (10 Hz side) control part based on VSG control. The Input side control (60 Hz side) composed of outer and inner controllers. The outer controller is shown on the left-hand side of Fig. 3.4, which controls the input active and reactive power (P_{60Hz}, and Q_{60Hz}) using a proportional and integral (PI) controller to produce the dq axis reference currents i_d^* and i_q^* according to

$$i_d^* = \left(k + \frac{k_i}{s}\right)\frac{(P^* - P_{60Hz})}{v_d} \tag{3.1}$$

$$i_q^* = \left(k + \frac{k_i}{s}\right)\frac{(Q^* - Q_{60Hz})}{v_d} \tag{3.2}$$

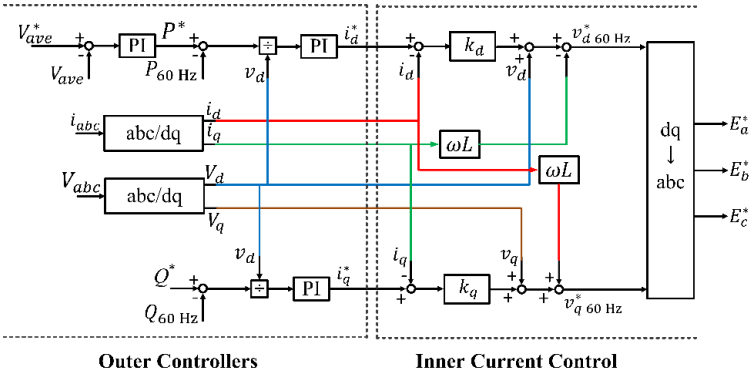

Fig. 3.4 A block diagram of the modular multilevel matrix converter (M3C) 60 Hz side conventional control.

The inner current controller (on the right-hand side of Fig. 3.4) tries to track the reference currents using a proportional gain. This controller provides the voltage vector references $v_{d\ 60Hz}^*$ and $v_{q\ 60Hz}^*$ as follows

$$v_{d\ 60Hz}^* = k_d(i_d^* - i_d) - \omega L i_q + v_d \tag{3.3}$$

$$v_{q\ 60Hz}^* = k_q(i_q^* - i_q) + \omega L i_d + v_q \tag{3.4}$$

The voltage vector references are transformed into three phase-to-neutral values E_{abc}^* using an inverse park transformation with a phase-locked-loop (PLL).

It is noteworthy to mention that each H-bridge cell contains a capacitor which acts as a dc voltage source, and the cell capacitor voltage must be kept almost constant around its given reference value. If this voltage value changes, it affects the output voltage of the low-frequency side as well as harmonic waveforms. Therefore, a capacitor average voltage deviation ΔV_{ave} control loop is employed to calculate the reference power command for the input side (60 Hz side) automatically by using the capacitor average voltage deviation and a PI controller. The capacitor average voltage V_{ave} is calculated from all the H-bridge cell capacitor voltages using (3.5),

$$V_{ave} = \frac{1}{N}\sum_{i=1}^{N} V_{cap\_i} \tag{3.5}$$

where V_{cap_i} is the capacitor voltage of the i_th cell and N is the total number of cells. A three phase-to-neutral voltage references are obtained through an inverse dq transformation as shown in Fig 3.4.

To determine the pulse width modulation (PWM) pattern from the voltage references, the space vector pulse-width modulation (SVPWM) control scheme is used. The capacitor in each H-bridge cell is regarded as a voltage source and various line-to-line voltages can be realized by the combination of the output voltages of these cells [4], [5].

The 10 Hz-side controller is implemented by using the VSG control system, which is divided into two parts, active power control and reactive power or output voltage control. Finally, the phase angle θ_m obtained from the VSG control is used to form the three reference phase voltages in the SVPWM.

3.3.2 VSG Control

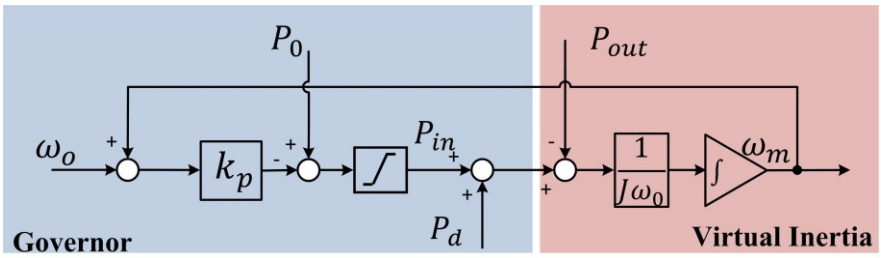

Fig. 3.5 VSG control scheme combines: Swing equation, damping power, and speed governor.

The VSG control is applied in both terminals, which is shown in Fig. 3.5. The control scheme concept of VSG is based on the swing equation of the synchronous generator, which is explained in Chapter 2. The VSG control enables the converter in a multi-terminal system to control power flow and share active and reactive power. To operate the LFAC two-terminal system, each terminal receives the gate signal for the IGBT switches following the amount of transmitting power as reference power from one terminal and the second terminal can receive the power automatically along with the synchronization of both terminals' power direction with the 10 Hz frequency on the low frequency side via VSG control scheme.

The VSG control is employed here to control the amount and the direction of the transmitted active power and to synchronize the transmitting frequency between the terminals. In the VSG control block shown in Fig.3.5, the swing equation is

$$P_{in} - P_{out} + P_D = J\omega_0 \frac{d\omega_m}{dt} \tag{3.6}$$

The swing equation is integrated using input variables P_{in}, P_{out} and P_D, which are input power, output power, and damping power, respectively. The inertia of rotating mass J shown in equation (3.6), which is determined as

$$J = \frac{MS_{base}}{\omega_0^2} \tag{3.7}$$

where, M is the inertia time constant. As a result, the virtual machine angular speed ω_m is obtained as

$$\omega_m = \frac{1}{J\omega_0} \int (P_{in} - P_{out} + P_D) dt \tag{3.8}$$

A phase-locked loop (PLL) is used to provide the measured output frequency in order to create the damping power P_D for the swing equation (3.8), as follows

$$P_D = D\left(\omega_m - \omega_g\right) \tag{3.9}$$

where D is the damping factor, which can be set as a small value while tuning.

The obtained virtual angular frequency ω_m is then integrated to generate the phase angle θ_m to be utilized afterwards by the inner controller of the M3C. The parameter design of the VSG control part is shown in [6], [7].

On the 60 Hz side, a conventional control is applied, which is discussed in Chapter 2 in details. It involves the active and reactive power of the 60 Hz side (P_{60Hz} and Q_{60Hz}). The cell capacitor voltage must be kept almost constant around its given reference value. If this voltage value changes, it affects the output voltage of the low-frequency side as well as harmonic waveforms. Therefore, instead of directly controlling the active power of the 60 Hz side (P_{60Hz}), the average capacitor voltage V_{ave} that is calculated from all the H-bridge cell capacitor voltages using (3.5) is controlled to be kept constant at reference V_{ave}^*. Then, a three-phase line-to-line voltage references for two sides are obtained through the inverse dq transformation.

Finally, both the VSG and the conventional controller outputs generate the reference voltage to be used later in the space vector pulse width modulation scheme (SVPWM). The SVPWM control scheme is employed for the M3C to control the output voltage and active and reactive power of both commercial (60 Hz) and low frequency (10 Hz) sides as well as to balance the H-bridge cell capacitor voltages [8], [9].

3.3.3 Governor Droop Controller

The concept of governor control, which has $\omega - P$ droop characteristics, is shown in Fig.3.3 and its control block is shown in Fig.3.5 in the governor part of the VSG control.

According to Fig.3.5, and in order to balance the power between P_{in} and P_{out}, the generator increases its power injected to the network when the network frequency is lower than the nominal frequency (10 Hz) according to

$$P_{in} = P_0 - k_p(\omega_m - \omega_0) \tag{3.10}$$

The governor control block which is shown in Fig.3.5, consists of a reference input power P_0 and output of the governor is then used as input power P_{in} in the VSG. The governor can synchronize the frequency in the two terminals. The governor compares measured frequency ω_0 to a given reference frequency ω_0 and generates the proper reference input power P_{in} injected to the VSG. k_p, is the droop coefficient which is chosen to allow 5% frequency variation for 1 pu power change.

3.3.4 Voltage and Reactive Power Control

As illustrated in the control block shown in Fig. 3.3, the output voltage is controlled in order to minimize the reactive power and keep the voltage unchanged in the steady-state. This is accomplished using Automatic Voltage Regulator (AVR) for one terminal (M3C 1), and the Automatic Reactive Power Regulator (AQR) for the other terminal (M3C 2) as shown in Fig 3.6 (a) and (b) respectively. In the AVR, the voltage reference V_0 is the line-to-line RMS value of the M3C low-frequency side output voltage, which may be a different value for each converter even in steady-state due to the line voltage drop. Q_0 is the reference reactive power of the LFAC transmission line.

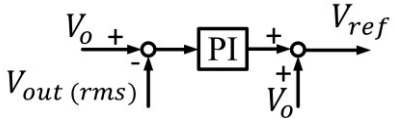

(a)

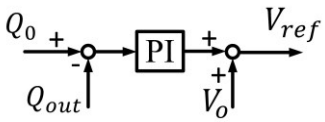

(b)

Fig.3.6 (a) Automatic Voltage Regulator (AVR) and (b) Automatic Reactive Power Regulator (AQR).

The reference output voltage V_{ref} should be regulated based on either AVR or AQR. The regulated output voltage will then be used as an input to the inner controller of the M3C.

3.4 Simulation Results

A simulation system has been implemented in PSCAD software to verify the proposed control scheme. The circuit configuration of simulation is shown in Fig. 3.1. The two-terminal system is driven by an M3C, and each M3C has 9 arms and each arm has 4 H-bridge cells connected in series (9-level) that interconnects the 60 Hz power system with LFAC transmission line. The VSG control is applied to the two M3Cs for low-frequency side.

Two terminal model configuration, which represents the M3C-LFAC system, is investigated. The command for power flow control is summarized in Table 3.1 as well as the main parameters of the numerical simulation.

Table 3.1 Parameters of M3C-LFAC system

Common Parameters	
Parameter	Value
Rated M3C power S_{M3C}	200 MVA
$V_{base_{LFAC}}$	275 kV
f_{LFAC}	10 Hz
f_{grid}	60 Hz
X_{grid}	0.1 pu
X_{LFAC}	0.016 pu
M3C Parameters	
Parameter	Value
Sampling frequency	2 kHz
Capacitor voltage	128 kV
Cell capacitor	0.69 s
Arm inductor	0.008 pu
AQR *and* AVR PI Controllers Parameters	
Parameter	Value
K_p	0.2 pu
K_i	0.5 s
VSG Parameters	
Parameter	Value
V_{base}	275 kV
P_{0_pu}	1 pu
ω_0	62.8315 rad/s
M	8 s
D	10 pu
k_{p_pu}	20 pu

A sampling frequency of 2 kHz is set. A capacitor in each cell works as a dc voltage source controlled by the inner controller of the M3C. The dc capacitor voltage is 128 kV and the time constant is 2 s. The transmission distance is 200 Km. The transmission cable is modelled by using a single-core XLPE land power cable from ABB [10]. In order to test the proposed system and the control scheme, the active and reactive power were shared between the terminals and through the 200 km transmission line. The amount

and direction of power were assumed at one terminal and the second terminal was commanded follows the command automatically and autonomously. With the help of the VSG control, the simulation conditions are as follows; the power flow from terminal 1 to terminal 2 is given to terminal 1 only, and it varies from the rated power of 200 MW for sending to the rated power of -200 MW for receiving by a step change of 100 MW at every 5 s. Fig. 3.7 (a) and (b) show active and reactive power of the low-frequency side of terminals 1 and 2, respectively. Fig. 3.7(c) shows the rms voltage waveforms of the low-frequency side of terminals 1 and 2, respectively.

Fig. 3.7(d) shows the virtual angular frequency of each terminal at the 10 Hz side. It is seen that the angular frequency deviates during each dynamic state and returns to its steady-state after a short time. The settling time is almost the same, and it depends on the inertia constant *M*.

Fig. 3.7(e) shows the capacitor average voltage of M3C 1. The active power command is determined from the capacitor average voltage deviation in the conventional controller of both M3Cs to control the active power of the 60 Hz side in order to minimize the harmonics and to output a constant low-frequency side voltage. Both capacitor average voltages were given command of 128 kV, and it can be seen from the figure that the capacitor average voltage was kept almost constant at the reference voltage of 128 kV, except for the transient period after the power reference was changed.

The output voltage and the reactive power were regulated by the AVR and the AQR, respectively. From Figs. 3.7 (b) and (c), it can be noticed that with these controllers, the reactive power of M3C1 changes in order to regulate the output voltage of that particular M3C. Whereas, on the other hand, the voltage is changed in order to properly regulate the reactive power of M3C by the act of the AQR.

It is confirmed that the entire system was successfully able to control active and reactive power flow and to keep the reactive power constant, and finally, it is confirmed that the proposed power control for the two-terminal LFAC using VSG control has proved its worthiness.

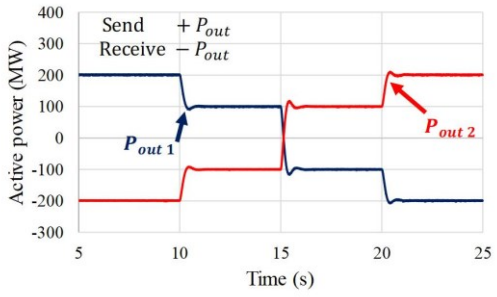

(a)

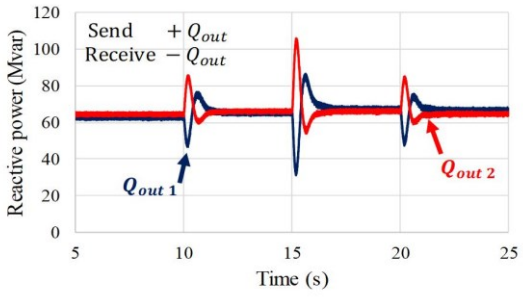

(b)

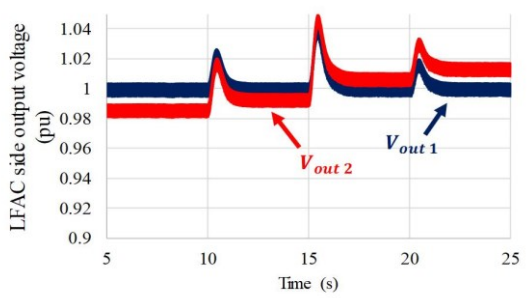

(c)

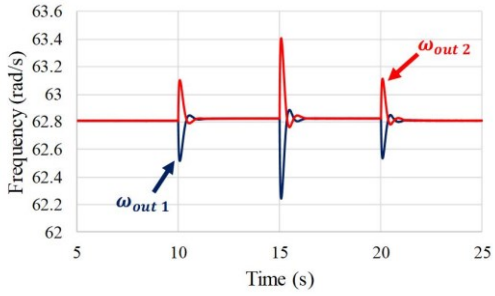

(d)

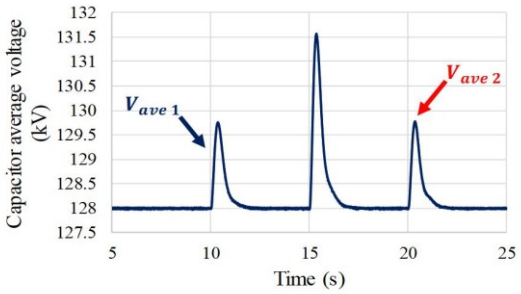

(e)

Fig. 3.7 Simulation results of; a) Active power, (b) Reactive power, (c) LFAC output voltage, (d) frequency, and (e) M3C 1 cell capacitor average voltage.

3.5 Summary

This chapter describes and validates a proposed control scheme of M3C for the two-terminal LFAC system with special focus on the advantages of using the M3C and VSG in LFAC transmission.

The proposed control scheme has been verified by simulation results of a two-terminal based VSG control and 9-level M3C model. The proposed control scheme that was explained in details is suitable for synchronized low frequency, regulating voltage and reactive power by integrating the VSG, and governor control for a large distance of transmission line.

Moreover, a brief discussion on the criteria of selecting the operating frequency and the outcomes of selecting a 10 Hz or 20 Hz frequency is shown, in which it needs to be put into account when designing the LFAC system.

References

[1] Pichetjamroen, A.; Ise, T. Power Control of Low Frequency AC Transmission Systems Using Cycloconverters with Virtual Synchronous Generator Control. *Energies* 2017, *10*, 1–13.

[2] Pichetjamroen, A.; Ise, T. A Proposal on Low Frequency AC Transmission as a Multi-Terminal Transmission System. *Energies* 2016, *9*, 687.

[3] Liu, S.; Wang, X.; Meng, Y.; Sun, P.; Luo, H.; Wang, B. A Decoupled Control Strategy of Modular Multilevel Matrix Converter for Fractional Frequency Transmission System. *IEEE Trans. Power Deliv*. 2017, *32*, 2111–2121.

[4] Kammerer, F.; Kolb, J.; Braun, M. A novel cascaded vector control scheme for the modular multilevel converter. In Proceedings of 37th Annual Conference of the IEEE Industrial Electronics Society (IECON), Melbourne, Australia, 7–10 Nov. 2011.

[5] Miura, Y.; Mizutani, T.; Ito, M.; Ise, T. Modular multilevel matrix converter for low frequency AC transmission. In Proceedings of the IEEE 10th International Conference on Power Electronics and Drive Systems (PEDS), Kitakyushu, Japan, 22–25 April 2013; pp. 1079–1084.

[6] Liu, J.; Miura, Y.; Ise, T. Comparison of Dynamic Characteristics Between Virtual 610 Synchronous Generator and Droop Control in Inverter-Based Distributed Generators. *IEEE* 611 *Trans. Power Electronics*, 2016, *31*, 3600-3611.

[7] Liu, J.; Miura, Y.; Ise, T. Fixed-Parameter Damping Methods of Virtual Synchronous Generator 623 Control Using State Feedback. *IEEE Access*, 2016, *7*, 99177-99190.

[8] Yushi Miura, Tomoya Mizutani, Michitaka Ito and Toshifumi Ise, "Modular Multilevel Matrix Converter for Low Frequency AC Transmission," 2013 IEEE 10th *International Conference on Power Electronics and Drive Systems (PEDS).* Pages: 1079 – 1084.

[9] Wataru Kawamura, Kuan-Liang Chen, Makoto Hagiwara, and Hirofumi Akagi," A Low-Speed, High-Torque Motor Drive Using a Modular Multilevel Cascade Converter Based on Triple-Star Bridge Cells (MMCC-TSBC)," *IEEE trans. on industry applications,* vol. 51, no. 5, September/October 2015.
[10]XLPE Land Cable Systems User's Guide. Available online: https://library.e.abb.com/public.

Chapter 4

Multiterminal Low Frequency AC Configuration Operation Using Modular Multilevel Matrix Converter and Virtual Synchronous Generator Control

4.1 Introduction

In this chapter, a new control scheme for the LFAC transmission system is presented in order to extend the point-to-point concept to form a multi-terminal LFAC (MT-LFAC) system, which has not yet been reported before in the literature. This configuration is meant for applications that require interconnection of remote power systems operating in nominal frequency via LFAC transmission lines. The MT-LFAC system considered as an alternative solution along with the conventional HVAC and MT-HVDC systems can offer attractive advantages.

In terms of controlling the M3C in an LFAC system, previous control methods such as [1] represent the state-of-the-art. A land located M3C is proposed to interface an LFAC system connecting an offshore wind farm with an onshore grid, and the M3C is controlled as a voltage source using a decoupled control strategy. Since there are no previous works on forming the MT-LFAC system interconnecting remote areas, if the system is selected to be controlled based on state-of-the-art solutions like [1], it will be required to apply the same control scheme as a master terminal, and control the other terminals as slave terminals. The reliability of such a system will be determined by the master terminal, and the power flow control can only be performed in a centralized manner, which requires communication. Moreover, there are some interactions between active and reactive power control loops due to the lower inductive line impedance of the LFAC system.

The virtual synchronous generator (VSG), sometimes called synchronverter, is a solution to provide synchronization power and inertia feature to power converters [2], [3]. The VSG control method introduces the well-known dynamic response of a synchronous generator (SG) [4], [5]. The VSG incorporated in the LFAC system is based on the SG swing equation and provides a virtual inertia support

in addition to the frequency regulation support. The virtual inertia is a property that enhances the LFAC system stability.

The integrated power angle provided by the VSG control can guide the operation of a multi-terminal system by controlling the amount and the direction of the active power autonomously and automatically. Thus, there is no need to use communication tools to synchronize the terminals. The VSG control allows the M3C to behave as an SG, thus contributing inertia and damping properties to the converter, as a result of the multi-terminal system operation. Moreover, the VSG control is equipped with voltage regulation control represented by either an automatic voltage regulator (AVR) or automatic reactive power regulator (AQR) to regulate the voltage and reactive power, respectively. The conventional VSG control is used for distributed generators [6], and the HVDC system is used to support a weak AC grid [7]. However, these studies are only focused on stabilization of ac grids and are not applied to the LFAC network.

The main contributions of this chapter can be summarized as follows:

(1) To form the proposed MT-LFAC electrical energy system, M3Cs are operated to convert the conventional frequency to low frequency with improved output waveforms on both sides.
(2) The used M3Cs are controlled by the VSG-based control to enable power-sharing and frequency stability in the LFAC network. The autonomous feature of the VSG control made the LFAC system more reliable and less communication-dependent in comparison to the existing master-slave control for point-to-point LFAC system.
(3) A new $\omega - P$ droop control scheme is proposed to allow the system to operate in both the commanded mode and the frequency restoration mode. Hence, the system can selectively work with/without local command while ensuring that no frequency deviation occurs in the steady-state.
(4) To address the concern of less inductive line impedance, the virtual inductive impedance is applied to ensure the decoupling between active and reactive power in the less inductive LFAC system.

4.2 Multiterminal Configuration Description

The configuration of the multi-terminal system studied in this work is shown in Fig. 4.1. It is a combination of three terminals; each terminal is driven by an M3C that acts as a frequency synthesizer to convert the 60 Hz power to 10 Hz.

All terminals' converters have the same control structure in which is combined of two parts; the 60 Hz side and 10 Hz side control. The 10 Hz side employs a VSG control to control the power of the low-frequency side. The 60 Hz side active and reactive power control uses a conventional control, with the outer and the inner current controllers on dq coordination frame.

Fig 4.1 shows an example of the MT-LFAC system with 275 kV, and 200 km LFAC transmission lines (parameters are chosen based on the XLPE land cable data sheet provided by ABB group, Power and automation technologies, Zurich, Switzerland) [8]. The RMS value of the voltage is chosen in order to ensure lower transmission line losses, with consideration of the withstand voltage of power semiconductor devices.

The role of the VSG control in the MT-LFAC system is achieved by using its swing equation in which it compares both input and output power of each terminal and thus produces the required phase angle accordingly. The obtained phase angle is used to provide the switching pulses for the M3C. More details of the proposed VSG control for the MT-LFAC system are explained in Section 4.3.1.

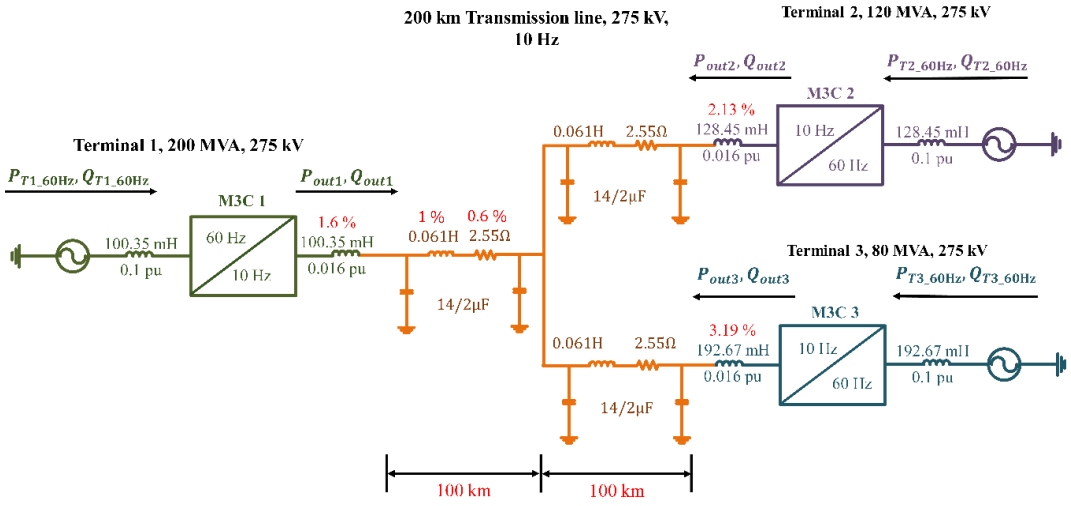

Fig. 4.1 Single line diagram of a multi-terminal low-frequency ac (MT-LFAC) system circuit configuration (pu values are calculated based on self-power rating of each terminal).

4.3 M3C Control

The main controller of M3C is shown in Fig. 4.2. The M3C control consists of two parts, 60 Hz side part which is based on the capacitor average voltage and reactive power control using PI controllers on the dq coordination frame as explained in details in chapter 2. The LFAC side controller implements the VSG control system, which is divided into two parts, active power control and reactive power or output voltage control. Finally, the phase angles $\boldsymbol{\theta}$ obtained from the two controllers are used in the SVPWM along with a reference voltages, which are obtained separately from each side's controller.

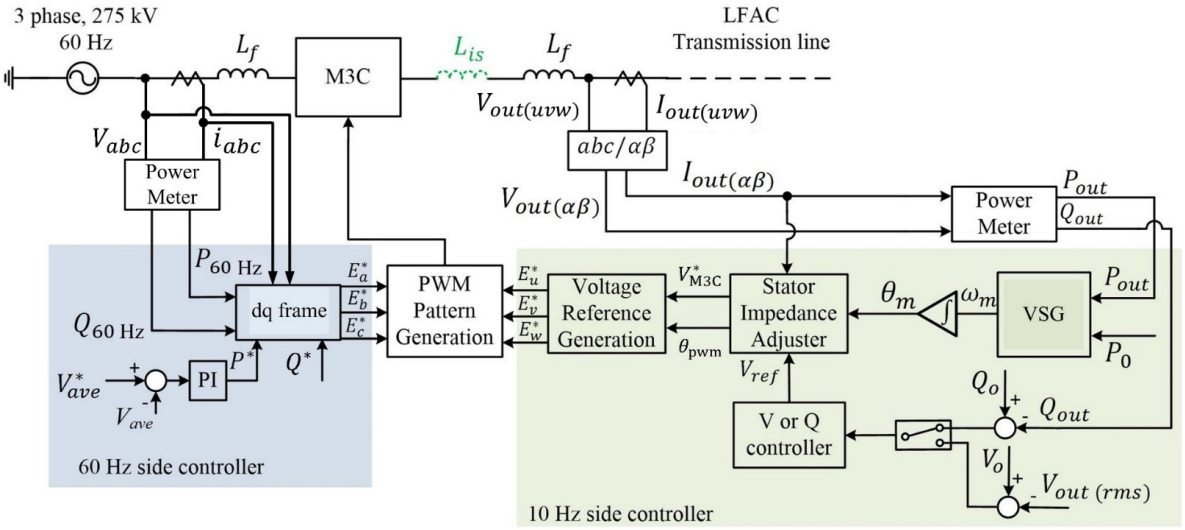

Fig. 4.2 Main control structure including the 60 Hz side power control and the 10 Hz side virtual synchronous generator (VSG) based control

4.3.1 VSG Control

The VSG control is used to control the amount and direction of the active power, and to synchronize, and stabilize the frequency among the terminals. The VSG control scheme that is used here is shown in Fig. 4.3. The VSG control scheme comprises the swing equation, the governor, and damping units. The swing equation of VSG is

$$P_{in} - P_{out} + P_d = J\omega_0 \frac{d\omega_m}{dt} \tag{4.6}$$

where ω_m is the virtual rotating angular frequency, ω_0 is the nominal frequency, and P_{in} ,P_{out}, P_d are the virtual shaft power produced by the governor control, the output power of the low-frequency side, and the damping power, respectively. J is the moment of inertia of rotating mass, which is determined as

$$J = \frac{MS_{base}}{\omega_0^2} \tag{4.7}$$

where M is the inertia time constant, and S_{base} is the rated power of each respective terminal.

The damping power P_d is generated by the state feedback control method [9] as follows

$$P_d = -k_{x\omega}(\omega_m - \omega_0) - k_{xP}\frac{1}{1+T_f s}P_{out} - k_{xi}\frac{1}{s}P_d \tag{4.8}$$

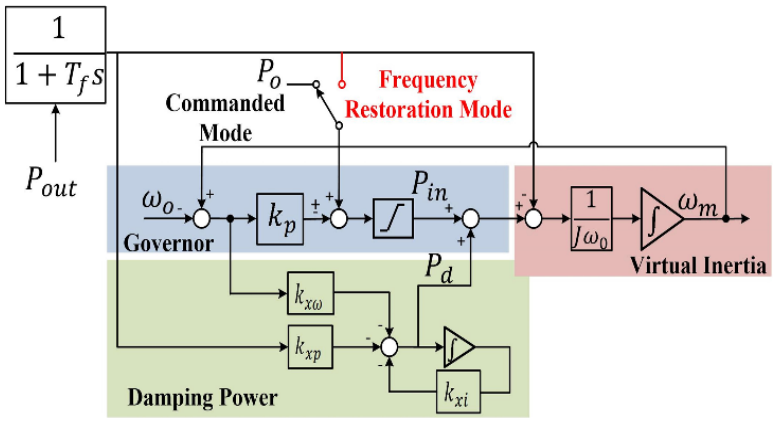

Fig. 4.3 Virtual synchronous generator (VSG) control combining the governor, damping power, and the virtual inertia control scheme.

where $k_{x\omega}, k_{xp}$, and k_{xi} are the feedback gains of virtual rotor frequency, output active power, and integral term of P_d, and T_f is the time constant of the low-pass filter (LPF), that is calculated based on

$$T_f = \frac{1}{2\pi f_f} \tag{4.9}$$

where, f_f is the cut off frequency. f_f =10 Hz is selected in order to attenuate the $2\omega_m$ ripples. This damping method technique is chosen because it can provide a fast response to power command change, and it can allow adding an LPF to filter the measured active power P_{out} in order to attenuate the ripples caused by the unbalance in the output voltage and/or current in the LFAC side. These ripples will affect the output power quality since they will enter the VSG control block. Moreover, the use of the Phase-Locked Loop (PLL) for detecting the grid frequency can be avoided, which is used in some previous works [10], [11]. All values are shown in Table 4.1. From (4.8), it can be noticed that the integral term of P_d exists, and this will force P_d= 0 in the steady-state. By rearranging (4.6), the virtual mechanical frequency can be rewritten as (4.10)

$$\omega_m = \frac{1}{J\omega_0}\int (P_{in} - P_{out} + P_d)\, dt \tag{4.10}$$

The obtained virtual angular frequency ω_m is then integrated to generate the phase angle θ_m to be utilized afterwards by the inner controller of the M3C. The parameter design of the VSG control part is shown in [6], [9].

4.3.2 Governor Control Types

The governor control part of the VSG, shown in Fig. 4.3, is based on the $\omega - P$ droop characteristic. It is preferable to use the $\omega - P$ droop control especially when the system is highly inductive like the traditional synchronous generator [12]. From Fig. 4.3, it can be noticed that there is a selector to decide the reference power term of the governor droop control. If P_0 is selected, the governor will operate in the commanded mode. On the other hand, if P_{out} is selected (where P_{out} is the low-frequency side online output power), a frequency restoration mode of operation will be performed.

The governor droop characteristic control has a conventional droop and reversed droop, as shown in Fig. 4.4. In the commanded mode, the virtual shaft power P_{in} is produced by the governor control as

$$\begin{aligned} P_{in} &= P_0 - k_p(\omega_m - \omega_0) \text{ (conventional)} \\ P_{in} &= P_0 + k_p(\omega_m - \omega_0) \text{ (reverse)} \end{aligned} \tag{4.11}$$

where P_0 is the commanded value of active power, which is set in per unit, ω_0 is the nominal frequency, and k_p is the droop coefficient which is proportional to the power rating of each corresponding terminal and is determined as follows:

$$k_{p\_pu} = \frac{k_p \omega_0}{S_{base}} \tag{4.12}$$

where, S_{base} is the power rating of each terminal. The adopted value $k_{p\_pu} = 20$ shown in Table 4.1 allows a maximum 5% frequency deviation during a 1.0 pu power transition, which is a typical value in the power system [9], [12], [13].

According to the droop characteristic illustrated by Fig. 4.4, Terminals 2 and 3 are assigned by a reverse droop control, compared to conventional droop in Terminal 1. This is achieved by assigning the droop coefficient k_p with a different sign. In Fig. 4.4, the subscript T_i indicates Terminal i (i = 1, 2, 3). In a multi-terminal system, the terminal designed to be the receiver can be assigned by a reverse droop while the terminal designed to be the sender can be assigned with the conventional droop control. It is noteworthy to mention that the power flow can also be from the receiver to the sender without any modification of droop characteristic. The k_p of all terminals remains unchanged throughout the simulation presented in Section 4.4.

From Fig. 4.3, when the frequency restoration mode of operation is selected, P_0 is substituted by P_{out}, thus Equation (4.11) becomes

$$P_{in} = P_{out} - k_p(\omega_m - \omega_0) \text{ (conventional)}$$
$$P_{in} = P_{out} + k_p(\omega_m - \omega_0) \text{ (reverse)} \tag{4.13}$$

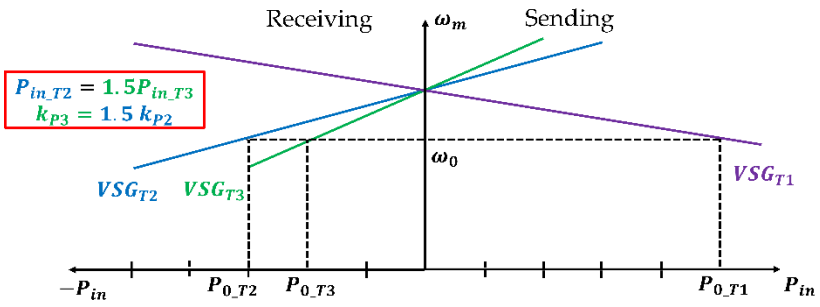

Fig. 4.4 Principle of conventional and reversed ω-P droop control.

By substituting (4.13) in (4.10)

$$\omega_m = \frac{1}{J\omega_0}\int \left(P_{out} + k_p(\omega_m - \omega_0) - P_{out} + P_d\right) dt$$
$$= \frac{1}{J\omega_0}\int \left(k_p(\omega_m - \omega_0) + P_d\right) dt \tag{4.14}$$

According to (4.14), it can be noticed that in the steady-state, the term $k_p(\omega_m - \omega_0) + P_d = 0$. As $P_d = 0$ in the steady-state [9], thus $\omega_m = \omega_0$. That is to say, the proposed control scheme allows the operator to smoothly restore the frequency in an MT-LFAC system. For the terminals operating in the commanded mode, as $\omega_m = \omega_0$, from (4.11), $P_{in} = P_0$. That is to say, the output power will follow the command accurately.

Finally, owing to the governor control, two objectives can be fulfilled. First, the system can operate under the frequency restoration mode, by that it senses the frequency variation of the network and decides the reference active power as given in (4.13). Secondly, based on (4.14), the frequency deviation restoration can be achieved.

4.3.3 Reactive Power and Voltage Control in Multiterminal System

In this model, the approaches taken to control the output voltage and reactive power are similar to the conventional ones in the HVAC system. Terminal 1 is set as a slack bus which is assigned to control the

voltage. Terminals 2 and 3 are aimed to control the reactive power by changing the output voltage. In other words, Terminal 1 is V-controlled (PV bus), whereas Terminals 2 and 3 are Q-controlled (PQ buses).

The reactive power control aims to control the low-frequency side output voltage profile that minimizes the active power losses of each terminal. This is accomplished by using an AVR with low-frequency side output voltage feedback or an AQR with low-frequency side output reactive power feedback as they are shown in the left side of Fig. 4.5. A selector is used in order to choose the method for controlling either the voltage or the reactive power. Terminal 1 is chosen to be responsible for controlling the output voltage by using AVR control. At the same time, Terminals 2 and 3 control the required reactive power to be provided for the transmission lines by using the AQR control. The AQR is a fixed type controller, which can follow a given command. The command of AQR in each terminal is set to provide reactive power consumed in the transmission line connected to this terminal, in order to minimize the reactive power in the LFAC system.

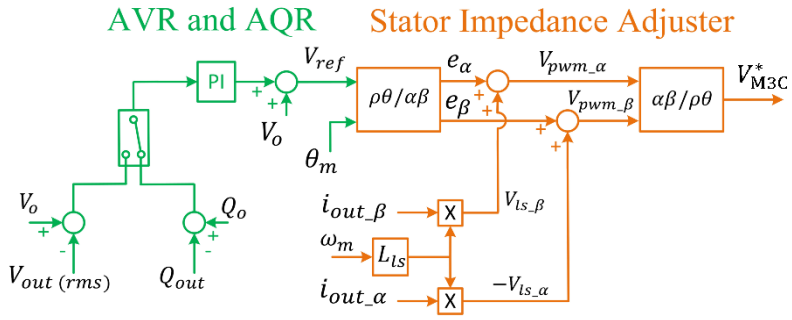

Fig. 4.5 Automatic voltage regulator (AVR), automatic reactive power regulator (AQR) and stator impedance adjuster block.

For the AQR control, because no reactive power transmission between the terminals is required in the MT-LFAC system, it is calculated and commanded in order to ensure the lowest possible losses, thus, a fixed reactive power value calculated from the reactance and capacitance values of the transmission line. After determining the reactive power for each terminal, the reference reactive power command can be set accordingly, which is shown by the AQR control block Q_0 in Fig. 4.5. From this figure, the resulted voltage V_{ref} is the RMS reference voltage, which will be updated by the virtual impedance control block.

4.3.4 Stator Impedance Adjuster

In this subsection, it is important to discuss the low-frequency transmission line *X/R* issue. Due to the low frequency used, the obtained *X/R* ratio will be 6 times smaller than that of the 60 Hz for a given rated voltage level, in which it is 1.5 in our case [14], [15]. Therefore, the system will become less inductive.

To solve the negative impact of this mentioned low *X/R* ratio, a virtual stator reactance is introduced to the VSG control to increase the total reactance of each terminal in order to avoid the coupling between *P* and *Q*. In [11], for a 60 Hz network, the total impedance X^* is set to 0.7 pu. In our work, the frequency difference is taken as criteria, thus the total impedance X^* is fixed at 0.1 pu, which is sufficient to make a larger *X/R* ratio, hence, to make the system inductive again. The total reactance X^* in pu according to the self-power rating is calculated as

$$X^* = \frac{XS_{base}}{V_{base}^2} = \frac{\omega_0(L_{ls}+L_f+L_{line})S_{base}}{V_{base}^2} = 0.1 \text{ pu} \tag{4.15}$$

where L_{ls} is the virtual stator inductance, L_f and L_{line} are the inductance of the L filter and the transmission line, respectively. From (4.15), L_{ls} is calculated as 0.089 pu for each terminal. Then, the reference voltage obtained from the AVR/AQR will be converted into a stationary frame, and this reference voltage will be updated according to the multiplication of the virtual stator inductor with the output current. Here, a stationary-frame based virtual impedance is applied owing to its simplicity and PLL-free nature. Then, the new reference voltage V_{M3C}^* will be realized and used for the SVPWM of the M3C.

4.4 Simulation Results

This section demonstrates the performance of the control system chosen to operate the MT-LFAC system and discusses different case studies applied to verify the proposed control approach used for the introduced case study. Furthermore, this section evaluates the VSG control scheme after transient events including the change of the power command and a power flow reversal, in addition to the transition of switching modes. The power flow algorithm and the case studies are implemented in PSCAD/EMTDC software environment.

The MT-LFAC system composed of three terminals, as shown in Fig. 4.1, was used for simulation. All terminals employ an M3C and a VSG control system. The terminals are connected via 200 km modelled as π −circuit transmission line. The transmission power cable parameters and other simulation parameters are shown in Table 4.1. The values of the PI parameters were manually tuned in per unit based on respective power or voltage ratings of each terminal.

Table 4.1. Simulation parameters.

Common Parameters			
Parameter	Value	Parameter	Value
V_{base}	275 kV	$X_{10\ Hz\ side}$	0.016 pu
f_{in}	60 Hz	Terminal 1 VA S_{base1}	200 MVA
f_{out}	10 Hz	Terminal 2 VA S_{base2}	120 MVA
$X_{60\ Hz\ side}$	0.1 pu	Terminal 3 VA S_{base3}	80 MVA
Modular Multilevel Matrix Converter (M3C) Parameters			
Parameter		Value	
Sampling frequency		2 kHz	
Capacitor voltage		128 kV	
Cell capacitor		470 µf	
Arm inductor		128 µH	
Virtual Synchronous Generator (VSG) Parameters			
Parameter	value	Parameter	Value
V_{base}	275 kV	ρ	0.29203
P_{0_pu}	1.0 pu	k_{xp}	1.0
ω_0	62.831 rad/s	$k_{x\omega}$	91.4140 pu
k_{p_pu}	20 pu	k_{xi}	8.8522 s^{-1}
M	8 s	T_f	0.0159 s
Automatic Reactive Power (AQR), and Automatic Voltage Regulator (AVR) PI Controller Parameters			
Parameter		Value	
K_p		0.001 pu	
K_i		0.5 s	
Transmission Line Parameters Cross-linked polyethylene (XLPE) Single core land cable			
Cross section		500 mm^2	
L		0.61 mH/km	
C		0.14 µf/km	
R		0.0255 Ω/km	

*The pu value in this table are based on self-power rating of each terminal.

Case 1: Terminal 1 Commanded Mode, Terminals 2 And 3 Frequency Restoration Mode

In this case, Terminals 2 and 3 were in the frequency restoration mode, and are controlled following a frequency variation in Terminal 1. This case is inverstigated instead of a full commanded mode system in order to confirm the VSG control robustness. This is done by setting a predefined reference power to the governor part of Terminal 1.

Fig. 4.6a demonstrates this case study, where the active power of three terminals is shown. The positive part indicates that power is being sent. Terminals 1, 2 and 3 were designed as 200 MVA, 120 MVA and 80 MVA, respectively. The scenario of command change sequence is as follows; at 0–15 s Terminal 1 is commanded to receive 200 MW from Terminals 2 and 3. At 15 s, Terminal 1 changes its command value to receive 100 MW. At 25 s, Terminal 1 starts to send 100 MW power instead of receiving it. Finally, at 35 s, Terminal 1 sends 200 MW to the Terminals 2 and 3. From Fig. 4.6a and according to the described scenario, the proposed control for the MT-LFAC system based on the governor $\omega - P$ droop control has been successfully performed with sharing power to Terminal 1 properly according to the power ratings of Terminals 2 and 3.

Figs. 4.6b, c show the reactive power and output voltage responses. The positive part indicates that the leading reactive power is provided by each terminal for the transmission line. Compared to the 50 Hz or 60 Hz conventional transmission lines, and according to Table 4.2, the numerical analysis shows that the reactive power was reduced almost 6 times in the case of the LFAC transmission system. Thus, by using the LFAC transmission, the main advantage of reduced losses can be achieved. Moreover, it was decided for Terminal 1 to control the output voltage whereas Terminals 2 and 3 are responsible for controlling the reactive power. Therefore, from Fig. 4.6c the output voltage of Terminal 1 was kept constant due to the AVR control. On the other hand, both voltages of T2 and T3 have similar deviations in voltage since they are controlled by AQR, thus, their terminal voltage is not directly controlled. However, the voltage sag is almost less than 3%, which is acceptable.

Table 4.2. Reactive power comparison.

Transmission Line Type	$\boldsymbol{Q_{out\_T1}}$ (Mvar)	$\boldsymbol{Q_{out_{T2}}}$ (Mvar)	$\boldsymbol{Q_{out_{T3}}}$(Mvar)
Low Frequency AC (LFAC)	64.472	65.765	66.168
High Voltage AC (HVAC)	385.895	393.656	396.077

Fig. 4.6d shows the virtual angular frequency of each terminal at the 10 Hz side. It is seen that the angular frequency deviates during each dynamic state and returns to its steady-state after a short time. The

settling time is almost the same, and it depends on the inertia constant *M*. Fig. 4.6e demonstrates the reason for choosing the inertia constant *M*. From the figure, it can be noticed that by increasing *M* the overshoot will be smaller with a longer settling time. When *M* is decreased, with a shorter settling time, overshoot becomes bigger, and larger ripples appeared in the response. Therefore, from the stability analysis point of view, M = 8 s is chosen considering a tradeoff between the transient performance (e.g., overshoot, settling time, and ripples).

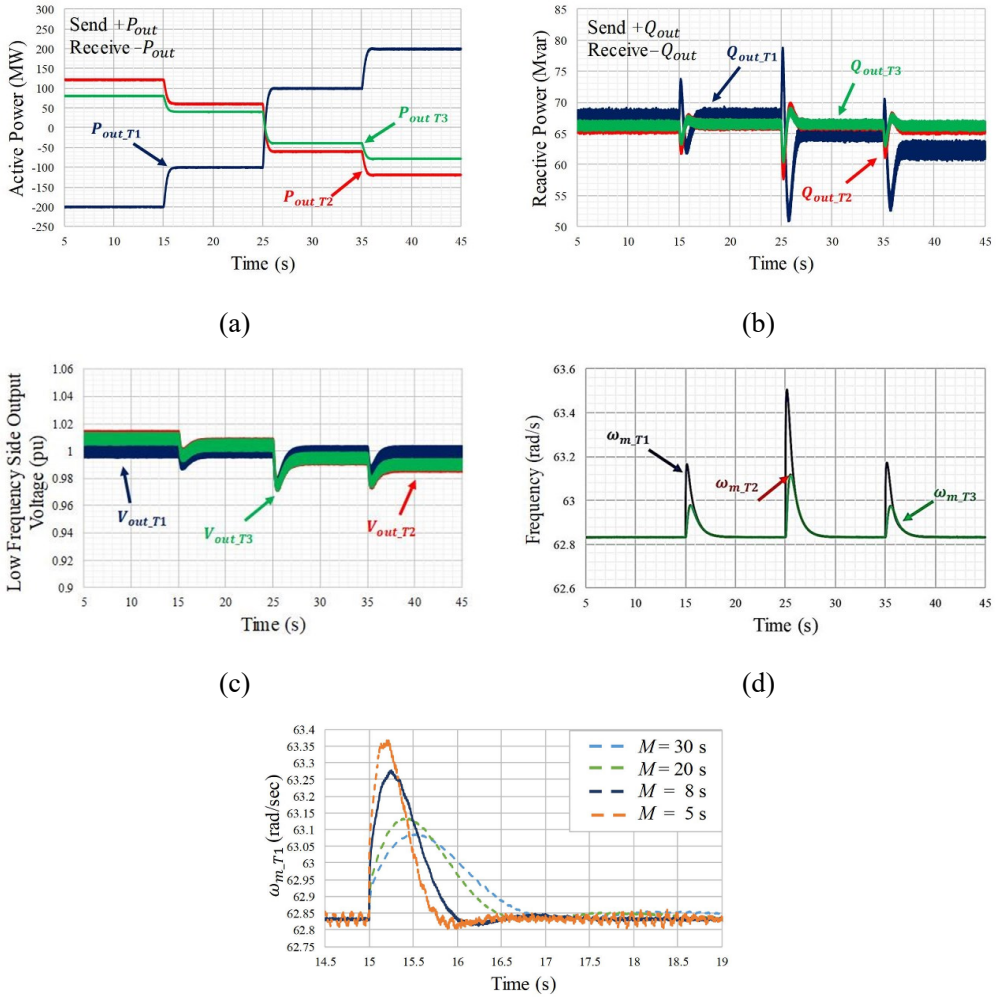

Fig. 4.6 System response for Case 1: (a) active power; (b) reactive power; (c) low frequency side voltage, and (d) frequency; (e) zoom of (d) of frequency deviations for various values of *M* for ω_{m_T1}.

In addition, in order to better interpret the performance of the M3C in the MT-LFAC system, simulation results are shown in Fig. 4.7 that demonstrate Terminal 1 M3C operation. Figs. 4.7a, b represent the 60

Hz side active and reactive power, and capacitor average voltage waveforms, respectively. After the transients are applied on the low-frequency side, the controllers of each corresponding M3C succeed in keeping the power balance between the input and output sides. This resulted in a constant capacitor average voltage waveform with only a small deviation (less than 0.5%) is obtained when the power command changes. Moreover, the power flow pattern on the 60 Hz side automatically follows the power flow change on the low-frequency side considering that the active power command of the 60 Hz side is set indirectly based on capacitor average voltage deviation. Figs. 4.7c, d show the 60 Hz and low-frequency sides' sinusoidal current and voltage zoomed in waveforms when the power reversal occurs at 25 s, which also follow the power flow patterns. It is clear that the M3C succeed in providing improved sinusoidal waveforms.

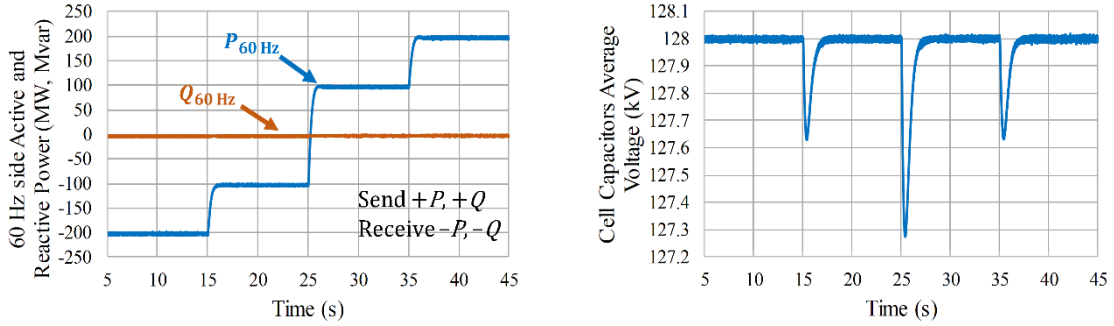

(a)

(b)

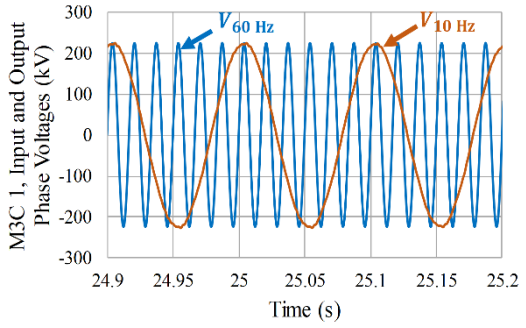

(c)

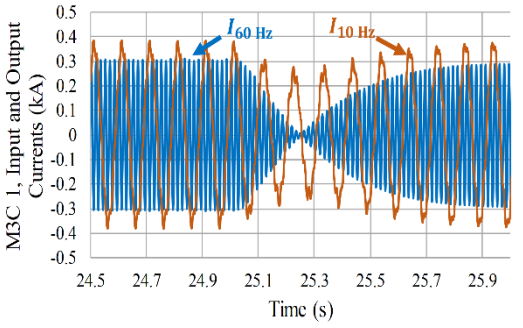

(d)

Fig. 4.7 M3C 1 response for Case 1: (a) 60 Hz side active and reactive power, (b) cell capacitors average voltage, (c) zoomed in, 60 Hz and low frequency sides' voltages, and (d) currents during power flow reversal.

Case 2 Terminals 1 and 2 Commanded Mode, Terminal 3 Frequency Restoration Mode

In this case, the proposed system is tested in order to confirm the flexibility of the proposed control system. Hence, Terminals 1 and 2 are in the commanded mode whereas Terminal 3 is in the frequency restoration mode. The dynamic scenario is divided into two parts. Referring to Fig. 4.8a, until 10 s, the commanded values to Terminals 1 and 2 are –150 MW (receiving) and 90 MW (sending), respectively. After 10 s, Terminal 2 power is increased to be 100 MW. As a result, Terminal 3 power is decreased based on the frequency restoration mode control. Finally, at 20 s, a full power reversal occurs. Hence, Terminal 1 starts to send the 150 MW while Terminals 2 (receives 100 MW) and 3 become receivers. The assumed operation can be successfully performed from Fig. 4.8a.

Figs. 4.8 b, c show the reactive power and the output voltage responses, respectively. The controller is the same as in Case 1. The difference in the AQR control is the reference command for the reactive power, which is also affected by the power change of the corresponding terminals. Moreover, since the AVR is used for controlling the voltage of Terminal 1, the reactive power of this terminal is not controlled at a specific value, thus it is dependent on the rest of the network. Oppositely, Terminals T2 and T3 are controlled by AQRs, thus their reactive power tracks respective reactive power command strictly, except transient condition.

Fig. 4.8 d, shows the output angular frequency of each terminal. Similar to Case 1, the frequency deviates after each power dynamic state and is promptly recovered due to the reverse droop control of the terminals against each other. Moreover, from the figure, at each dynamic state, firstly, the frequency of the master terminal changes. In response, the droop control of the terminal frequency restoration mode synthesizes this event and changes its frequency. Terminal 3 changes its power accordingly without causing any steady-state frequency deviation.

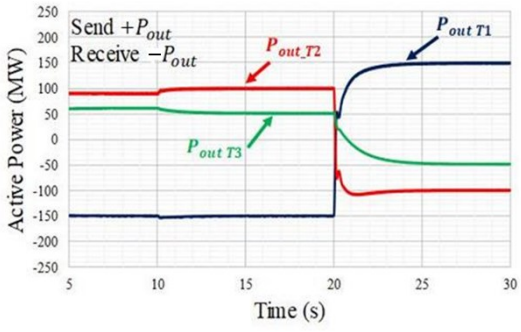

(a)

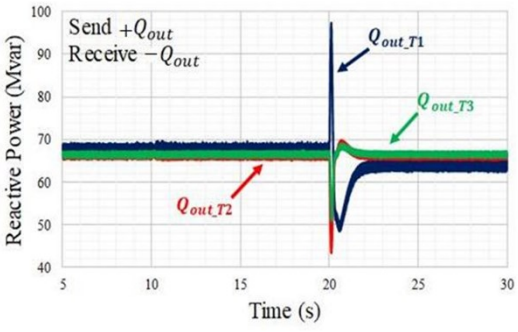

(b)

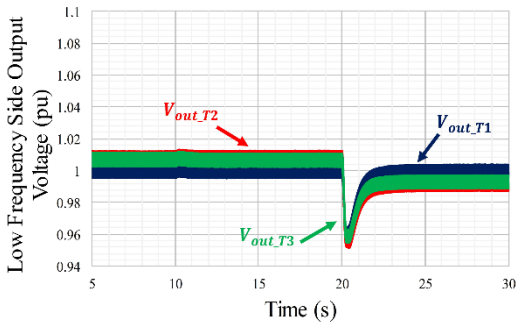

(c)

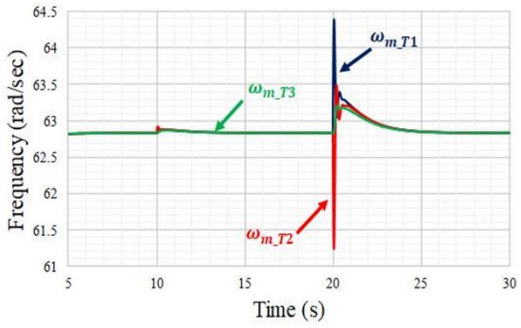

(d)

Fig. 4.8 System response for Case 2: (a) Active power; (b) reactive power; (c) low frequency side voltage and (d) frequency.

Case 3: Terminal 2 Switching from Commanded Mode To Frequency Restoration Mode

In this case, the proposed system is tested in a scenario including control mode transition. In this scenario as depicted in Fig. 4.9a, first, both Terminals 1 and 2 are operated in a commanded mode based on their respective power ratings, and Terminal 3 operates in the frequency restoration mode. Then, at t = 10 s, the switch of Terminal 2 shown in Fig. 4.3, changes from the commanded mode to the frequency restoration mode. It can be seen, during this mode transition, the power-sharing acts smoothly and remains constant. Thus, the VSG was able to guarantee a proper power-sharing without any dedicated communication channel. Thus, the scenario becomes the same as in Case 1 when Terminal 1 controls the power flow of the entire system by its commanded value. At t = 15 s, the command of Terminal 1 changes to receive 175 MW instead of 200 MW and based on the frequency restoration mode in Terminals 2 and 3, the power command was properly accommodated.

Fig. 4.9 b shows the output angular frequency of each terminal. It can be noticed that there is even no frequency deviation during the transition of the mode switching of Terminal 2. Similar to Case 1, the frequency deviates after 15 s and is promptly recovered due to the reverse droop control of the terminals against each other.

The system response shown in Fig. 4.9 demonstrates that, unlike the conventional frequency restoration method, the proposed frequency restoration mode can be started at different instants while keeping a reasonable power allocation.

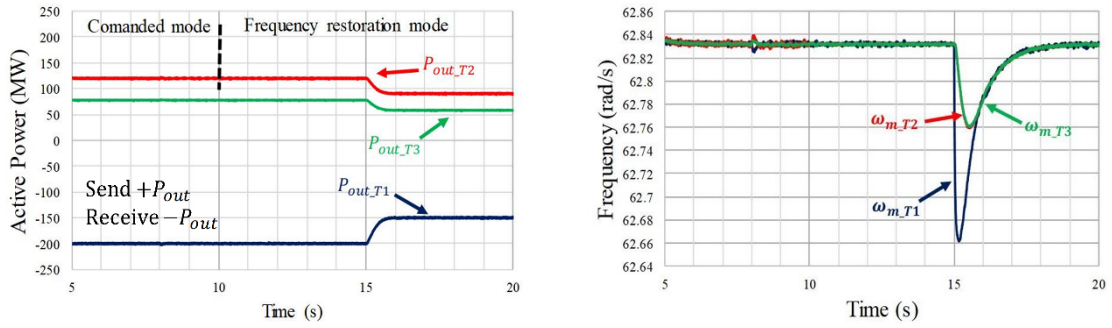

(a) (b)

Fig. 4.9 System response for Case 3: (a) Active power and (b) frequency.

4.5 Summary

In this chapter, a control scheme to form a multi-terminal low-frequency ac (MT-LFAC) system is proposed as an alternative solution to both multi-terminal high voltage DC (MT-HVDC) and high voltage AC (HVAC) systems in order to provide long-distance transmission to interconnect remote power systems. Characteristics of the proposed system are studied, and the obtained results are summarized as follows:

(1) Application of virtual synchronous generator (VSG) control in 10 Hz side was proposed in order to autonomously control active and reactive power and voltage of each terminal and maintaining the frequency stable in the steady-state.

(2) The VSG control used in this work has succeeded in enabling the M3Cs to behave like synchronous generators to construct the MT-LFAC network.

(3) Autonomous frequency restoration is realized by the proposed frequency restoration mode and the problem of the low *X/R* ratio in LFAC is solved by virtual impedance control.

(4) The control scheme proposed for the MT-LFAC system has proved its flexibility and its ease of implementation. Thus, the multiterminal system can be easily extended to more terminals without altering the controller coefficients and/or parameters since they are in per-unit values. The only point that needs to be considered in deciding the role of power flow, for example; each terminal capacity, sending vs. receiving groups of terminals, and the total amount of the power that needs to be accommodated.

References

[1] Liu, S.; Wang, X.; Meng, Y.; Sun, P.; Luo, H.; Wang, B. A Decoupled Control Strategy of Modular Multilevel Matrix Converter for Fractional Frequency Transmission System. *IEEE Trans. Power Deliv*. 2017, *32*, 2111–2121.

[2] Zhang, L.; Harnefors, L.; Nee, H.P. Power-synchronization control of grid-connected voltage-source converters. *IEEE Trans. Power Syst*. 2010, *25*, 809–820.

[3] Alipoor, J.; Miura, Y.; Ise, T. Power system stabilization using virtual synchronous generator with alternating moment of inertia. *IEEE J. Emerg. Sel. Top. Power Electron* 2015, *3*, 451–458.

[4] Zhang, L.; Harnefors, L.; Nee, H.P. Modeling and control of VSCHVDC links connected to island systems. *IEEE Trans. Power Syst*. 2011, *26*, 783–793.

[5] Bevrani, H.; Fracois, B.; Ise, T. *Microgrid Dynamics and Control*; Wiley: Hoboken, NJ, USA, 2017.

[6] Liu, J.; Miura, Y.; Ise, T. Comparison of Dynamic Characteristics between Virtual Synchronous Generator and Droop Control in Inverter-Based Distributed Generators. *IEEE Trans. Power Electron.* 2016, *31*, 3600–3611.

[7] Zhu, J.; Booth, C.D.; Adam, G.P.; Roscoe, A.J.; Bright, C.G. Inertia Emulation Control Strategy for VSC-HVDC Transmission Systems. *IEEE Trans*. *Power Syst*. 2013, *28*, 1277–1287.

[8] XLPE Land Cable Systems User´s Guide. Available online: https://library.e.abb.com/public (02/07/2019).

[9] Liu, J.; Miura, Y.; Ise, T. Fixed-Parameter Damping Methods of Virtual Synchronous Generator Control Using State Feedback. *IEEE Access* 2016, *7*, 99177–99190.

[10] Shintai, T.; Miura, Y.; Ise, T. Oscillation damping of a distributed generator using a virtual synchronous generator. *IEEE Trans. Power Del*. 2014, *29*, 668–676.

[11] Liu, J.; Miura, Y.; Bevrani, H.; Ise, T. Enhanced Virtual Synchronous Generator Control for Parallel Inverters in Microgrids. *IEEE Trans. Smart Grid* 2017, *8*, 2268–2277.

[12] Bevrani, H. *Robust Power System Frequency Control*, 2nd ed.; Springer: Berlin/Heidelberg, Germany, 2014.

[13] Sakimoto, K.; Miura, Y.; Ise, T. Stabilization of a power system including inverter-type distributed generators by a virtual synchronous generator. *Electr. Eng. Jpn. (Engl. Transl. Denki Gakkai Ronbunshi)* 2014, *187*, pp. 7–17.

[14] Ngo, T.; Lwin, M.; Santoso, S. Steady-State Analysis and Performance of Low Frequency AC Transmission Lines. *IEEE Trans. Power Syst*. 2016, *31*, 3873–3880.

[15] Tleis, N. *Power Systems Modelling and Fault Analysis*; Newnes Elsevier: Oxford, UK, 2008; pp. 616–618.

Chapter 5
Interconnection of Low Frequency AC System with a Remote AC Grid Using Dual Virtual Synchronous Generator Control-Based Modular Multilevel Matrix Converter

5.1 Introduction

In this chapter, another study of the proposed system focusing on the application of providing frequency regulation support for the LFAC system interconnecting a remote ac grid to the main grid using M3Cs as ac/ac converters. This is realized by using a dual VSG control for the M3C at the remote ac grid side. Each VSG has a different task. The LFAC side VSG provides a synchronized power for the LFAC network to enable a potential multi-terminal operation as demonstrated in chapter 4 and in [1]. Moreover, it maintains the cell dc capacitor voltage constant. Meanwhile, the remote ac grid side VSG is employed to enable the converter to mimic the dynamics of the SG and thus to provide a robust frequency regulation support for the remote ac grid. The concept of this work is stimulated by the works on the VSC-HVDC system with the inertia emulation [2]; however, the feature of our proposed M3C-LFAC system removes the limitations of using an HVDC transmission system. In other words, this work can be used as an alternative solution for better providing the existed services by the HVDC system.

It is noteworthy to mention that applying a dual VSG for controlling both M3C sides is not straightforward. Due to the intentional slow response of VSG control in both sides, it is difficult to apply conventional average dc capacitor voltage control, which requires a fast inner current control loop. Therefore, in this work, an average dc capacitor voltage versus active power (V_{ave}-P) droop control method integrated into the LFAC side VSG control is proposed, to achieve the balance between input and output M3C active powers and thus to maintain the capacitor voltage while reacting fast enough to support the dynamics of a remote ac grid. Such control technique has never been applied, particularly with the VSG for M3C control.

5.2 Issues Associated with Remote AC Grid

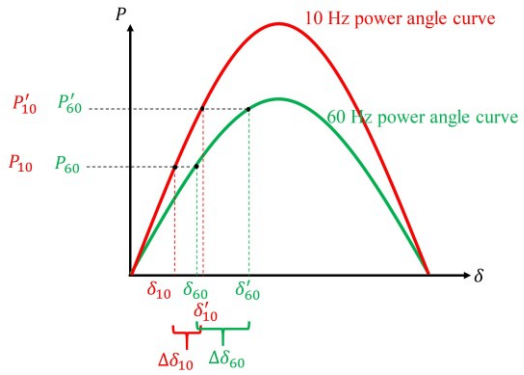

Fig. 5.1 Power angle curve comparison

In addition to the well-known disadvantages of the conventional ac system, in Fig. 5.1 two essential facts are demonstrated;

1- The advantage of using the LFAC system and its impact on the power angle curve as well as the maximum power transfer.

2- The weakness of the conventional frequency transmission system during transient-state can be demonstrated by looking at Fig. 5.1 For the same amount of power change (which represents a transient state) both operating points of LFAC and conventional ac will move to a new location (from δ_{60}, and δ_{10} to δ'_{60}, and δ'_{10}, for conventional and LFAC, respectively), thus each power angle will change from δ to δ'. The power angle deviation is related to frequency according to

$$P = \frac{|E||V|}{X} sin\,\delta$$
$$X = 2\pi f \tag{5.1}$$

As a result, the rate of change of the power angle when operating with LFAC system ($\Delta\delta_{10}$) is less than when operating with a conventional ac system ($\Delta\delta_{60}$), which results in low transient stability curve and a long time for returning to steady-state.

In conclusion, the ac system transient withstands ability become weaker if the ac system with a low rating power is remotely connected, and if the penetration of inverter-based renewable energy is increased which causes system inertia to significantly decrease. Therefore, a frequency regulation scheme with extended transmission distance is required.

5.3 System Configuration

A case study of point-to-point M3C-LFAC configuration is presented in this chapter to demonstrate our proposed control scheme, which is illustrated in Fig. 5.2. It is a combination of two stations, and each station is driven by an M3C that acts as a frequency converter to convert the low-frequency ac (10 Hz) to 60 Hz in order to interface with the grid.

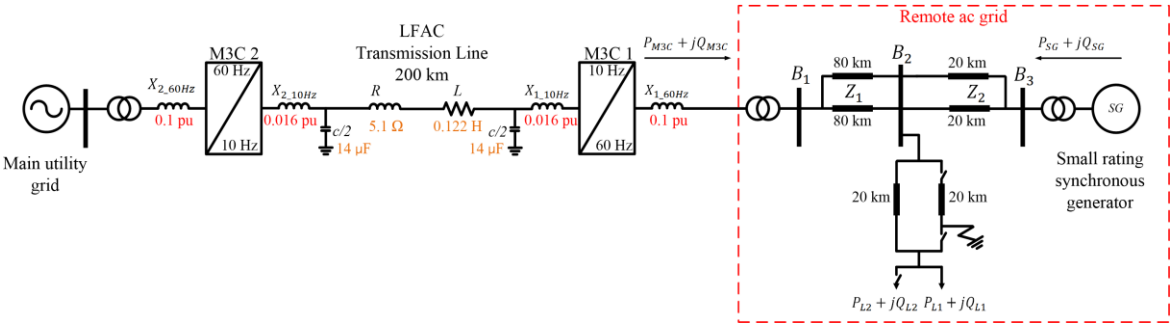

Fig. 5.2 Single-line diagram of a point-to-point M3C-LFAC system.

It is noteworthy to mention that this configuration can be easily extended to a multi-terminal LFAC system as proposed in chapter 4. The focal point of this chapter is the remote ac grid (60 Hz) side of M3C 1 as an interface to the LFAC system to show the advantages of the proposed control compared to the existing control schemes for M3C-LFAC system. Therefore, the control scheme of the main utility side M3C (M3C 2), which uses the existing control scheme of chapter 4, is omitted in this chapter.

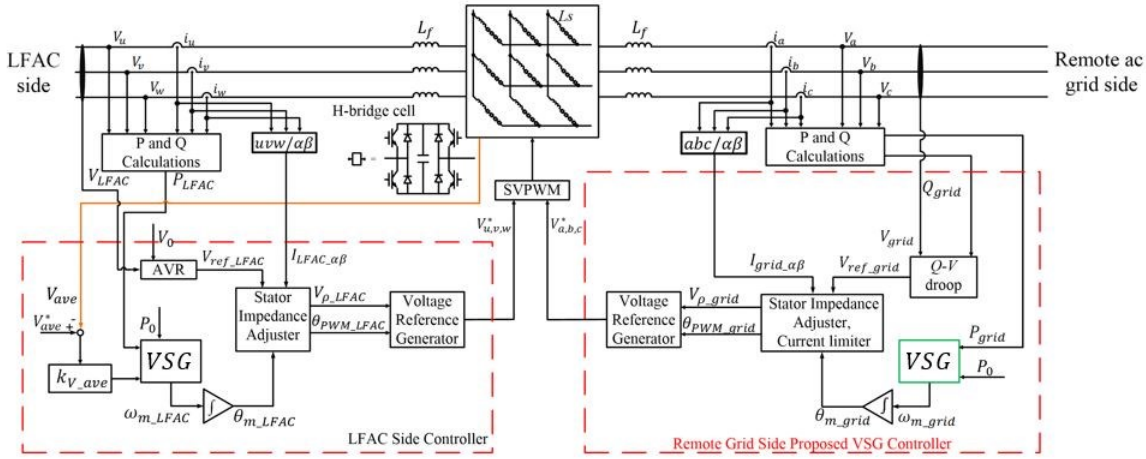

Fig. 5.3 Main circuit and the proposed control system of M3C 1.

5.4 Control Scheme

Fig. 5.3 shows the circuit configuration and the entire control scheme of M3C 1. The M3C circuit consists of nine arms, each arm has four H-bridge cells connected in series and these cells connect the grid side to the LFAC side. In practical application, each arm consists of hundreds of H-bridge cells considering the voltage level, thus the filter inductance L_f can be quite small. In this study, the number of cells is reduced to four for simplicity and less computational time of the simulation. Moreover, small inductors called arm inductors (L_s) are connected with each converter arm in order to suppress the current flowing at the timing of commutation between those arms. The overall control of the M3C is shown in Fig. 5.3. The control scheme can be divided into two parts; the grid side (60 Hz side) control part, and the LFAC side (10 Hz side) control part. From Fig. 5.3, the grid side is controlled by using either a VSG control or a conventional control based on PI controllers on the *dq* coordination frame as shown in details in Fig. 5.4.

5.4.1 Conventional Control of M3C

Fig. 5.4 shows the conventional remote ac grid side controller of the M3C that combines both the outer controller (on the left) and the inner controller (on the right). A synchronous *dq* reference approach is conventionally employed to guide the M3C control [3], [4]. A positive sequence of three-phase voltages V_{abc} and currents i_{abc} is transformed to the *dq* components using the Park's transformation, with the phase angle (θ_{PLL}) obtained from the PLL.

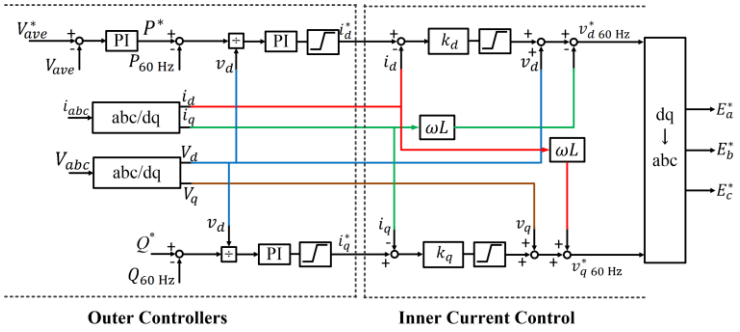

Fig. 5.4 A block diagram of the M3C remote ac grid side conventional control.

The outer controllers include controlling active and reactive power of the grid side. The active and reactive power that the M3C injects into the grid are expressed in dq-axis as

$$P_{60\,Hz} = \sqrt{2/3} * (v_d i_d + v_q i_q) \tag{5.1}$$

$$Q_{60\,Hz} = \sqrt{2/3} * (v_q i_d - v_d i_q) \tag{5.2}$$

Both active and reactive powers can be controlled using PI controllers on the *dq* coordinate in the outer controllers. However, to keep the active power balance between both sides, instead of directly controlling the active power, in [1], the average dc capacitor voltage V_{ave} is controlled, which is calculated from all the H-bridge cell capacitor voltages and is controlled to be kept constant at reference V_{ave}^*.

The outer controllers' task end at the points when the active power controller produces the d-axis current reference i_d^* and the reactive power controller produces the q-axis current reference i_q^*. The inner current control results in generating the voltage vector references v_d^* and v_q^* using proportional gains (k_d, k_q). Finally, these voltage references are transformed into a three-phase voltage references through inverse Park's transformation to be used later to determine the PWM pattern via a voltage space vector scheme.

This controller will be later replaced with a VSG control to compare their effectiveness on the remote ac grid. As for the LFAC side control, to form a multi-terminal LFAC system, the conventional one also uses a VSG control [1]; thus, it is almost the same as the proposed one shown in Fig. 5.3. However, since the average dc capacitor voltage V_{ave} is controlled by the remote ac grid side, which is shown in Fig. 5.4, the proposed average dc capacitor voltage control discussed afterwards is not applied. Therefore, it is much easier for the conventional method to apply the VSG control in the LFAC side.

5.4.2 Proposed Dual VSG Control

As shown in Fig. 5.3, which clearly demonstrates the feature of the proposed system, two VSG control units are used in both the LFAC and the remote ac grid sides. Each VSG comprises an active power-frequency (*P-f*) control part, and a reactive power control part. The M3C 1 employs a *Q-V* droop controller on its remote ac grid side, whereas an automatic voltage regulator (AVR) on its LFAC side. The *P-f* control part used for both LFAC and the remote ac grid sides of the M3C 1 is almost identical except that the droop characteristic between the average dc capacitor voltage and active power (V_{ave}-*P*) is included to be an additional part of the LFAC side VSG controller, as shown in Figs. 5.3 and 5.5. This design is made from the following two concerns; First, when the LFAC side active power includes the (V_{ave}-*P*) droop, the losses of the converter within the received power from the LFAC side will be included, otherwise, the system will experience an input and output power imbalance, which results in converter cell dc capacitor voltage deviation. Second, if the active power of the remote ac grid side is set indirectly, the remote ac grid side VSG controller will choose to regulate the cell dc capacitor voltage instead of grid power. Thus, the grid power transient response will be slower because the VSG controller of the remote ac grid side will take a longer time to realize and synthesize the power change in the remote ac grid. As a result, the system will fail to

support the dynamic state of the remote ac grid. In other words, the remote ac grid side VSG will not be able to quickly inject active power to mitigate the frequency deviation and the entire LFAC link will not be able to react fast to contribute to enhancing frequency regulation.

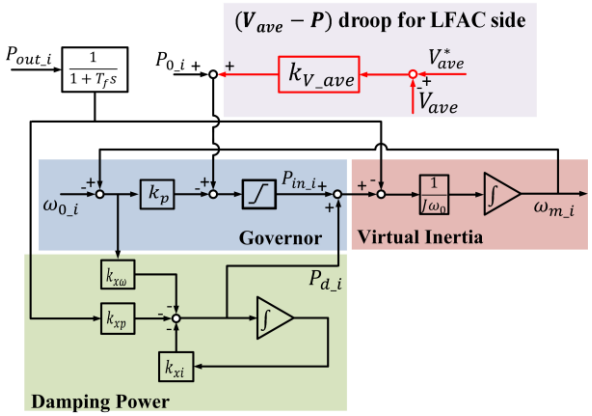

Fig. 5.5 Proposed VSG control combining the governor, damping power, and the virtual inertia control scheme, and V_{ave}-P droop (for LFAC side only).

The VSG parameters are input to the control scheme from those sides accordingly. It can be seen from Fig. 5.5, which represents the VSG control scheme where the input signals are included with the subscript *i*, referring to the LFAC or the remote ac grid side measured signals. The VSG control function comprises the swing equation, governor, and damping units. The swing equation of the VSG is

$$P_{in\_i} - P_{out\_i} + P_{d\_i} = J\omega_{0\_i}\frac{d\omega_{m\_i}}{dt} \tag{5.3}$$

where ω_m is the virtual rotating angular frequency, ω_0 is the nominal frequency, and P_{in} ,P_{out}, P_d are the virtual shaft power produced by the governor control, the output power, and the damping power, respectively. J is the moment of inertia of rotating mass, which can be determined as

$$J = \frac{MS_{base}}{\omega_0^2} \tag{5.4}$$

where M is the inertia time constant, and S_{base} *is* the rated MVA of the M3C.

The damping power P_d is generated by a state feedback control loop as follows [5]

$$P_{d\_i} = -k_{x\omega}(\omega_m - \omega_0) - k_{xP}\frac{1}{1+T_f s}P_{out} - k_{xi}\frac{1}{s}P_{d\_i} \tag{5.5}$$

where $k_{x\omega}$, k_{xp}, and k_{xi} are the feedback gains of virtual rotor frequency, output active power, the integral term of P_d; and T_f is the time constant of the low-pass filter (LPF), and VSG control parameters are given in Table 5.1. The used damping method allows the designer to avoid using the PLL for detecting the frequency, as applied in some previous methods [6], [7]. By rearranging (5.3), the virtual mechanical frequency is thus

$$\omega_{m\_i} = \frac{1}{J\omega_0}\int \left(P_{in\_i} - P_{out\_i} + P_{d\_i}\right) dt \tag{5.6}$$

where, the obtained virtual angular frequency ω_m is then integrated to generate the phase angle θ_{m_i} to form a three-phase reference voltage for the LFAC and the grid sides. The design of VSG control parameters is explained in [5], [8].

The governor control part of the VSG, shown in Fig. 5.5, is working based on the *ω-P* droop characteristic. It is preferable to use the *ω-P* droop control especially when the system is highly inductive like traditional SG. Moreover, conventional droop control is used for the sending terminal (M3C 2) whereas a reversed droop control is used for the receiving terminal (M3C 1) as explained in [1]. The conventional and reversed governor control produce the shaft power P_{in} as follows

$$\begin{aligned} P_{in} &= P_0 - k_p(\omega_m - \omega_0) \text{ (conventional)} \\ P_{in} &= P_0 + k_p(\omega_m - \omega_0) \text{ (reversed)} \end{aligned} \tag{5.7}$$

where P_0 is the commanded value of active power, k_p is the droop coefficient, and ω_0 is the nominal frequency [6], [9]. The droop coefficient is chosen to allow 5% change of frequency as a response to a full active power change and it was set in per unit value, calculated as

$$k_{p\_pu} = \frac{k_p\omega_0}{S_{base}} \tag{5.8}$$

5.4.3 Reactive Power and Voltage Profile Control Scheme

In order to give a detailed look at the other control parts in Fig. 5.3, this subsection discusses the output reactive power and voltage.

Fig. 5.6(a) represents the *Q-V* droop control on the remote ac grid side, whereas Fig. 5.6(b) represents the AVR of the LFAC side. The *Q-V* droop controller is preferable when two parallel distributed generators (DGs) are connected at the point of common coupling in order to share the reactive power autonomously.

The term "droop" is provided by the voltage difference block with a droop coefficient k_q that is selected to allow 10% variation when producing 1 pu reactive power block. $k_{q_{pu}}$ is defined as

$$k_{q\,pu} = \frac{k_q S_{base}}{V_{base}} \tag{5.9}$$

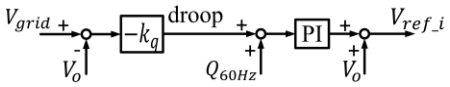

(a)

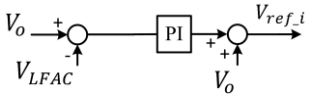

(b)

Fig 5.6 Control block of M3C 1 (a) Remote ac grid side *Q-V* droop block, (b) LFAC side AVR.

The AVR is used in the LFAC in order to maintain the voltage level by varying the reactive power. Whereas, the other terminal(s) in the LFAC network use an automatic reactive power regulation (AQR) in order to minimize the reactive power sharing errors, as shown in chapter 4.

The result of all controllers is $V_{ref\,i}$, (the subscript *i* refers to either remote ac grid or LFAC sides parameters of each M3C), which indicates the reference voltage generated from these controllers to be used later as an input to each corresponding stator impedance adjuster block as shown in Fig. 5.7 (a).

5.4.4 Stator Impedance Adjuster

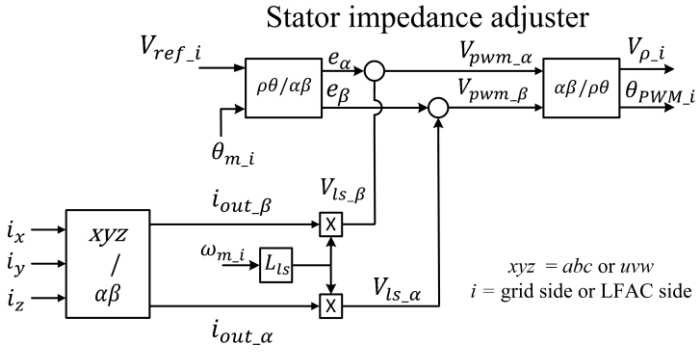

(a)

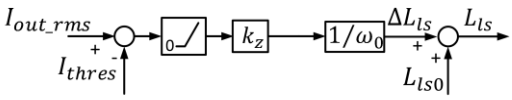

(b)

Fig. 5.7 M3C1 (a) Stator impedance adjuster, and (b) Current limiter control for remote ac grid side.

The stator impedance adjuster block is incorporated along with the dual VSG control in the M3C-LFAC system. Each one has a different function. For example, for the LFAC side, due to the low frequency, the *X/R* ratio will be 6 times smaller than that of the 60 Hz for a given rated voltage level, in which it is 1.5 in this system. Thus, the system will become less inductive [10]. Therefore, the virtual stator reactance is introduced to increase the total reactance of the M3C station in order to avoid the coupling between *P* and *Q*. Based on [7], a stator impedance control is applied to adjust the total output reactance of each terminal, which is calculated as

$$X^* = \frac{XS_{base}}{V_{base}^2} = \frac{\omega_0\left(L_{ls} + L_f + L_{line}\right)S_{base}}{V_{base}^2} \tag{5.10}$$

where, L_{ls} is the virtual stator inductance, L_f and L_{line} are the inductance of the L filter and the transmission line, respectively. From (5.10), L_{ls} is calculated as 0.089 pu for the LFAC side. Thus, the AVR output results are updated by the stator impedance adjuster block.

On the other hand, another function of the stator impedance is to be used to increase the converter's output impedance temporarily during an overcurrent condition (e.g. occurrence of fault) [11], [12], [13] as shown in Fig. 5.7(b). This function provides the fault ride-through (FRT) ability for a VSG control scheme, whereas, the FRT ability is realized by a current reference limiter in conventional control as shown in Fig. 5.4.

The idea of current limiting strategy is to promptly increase the virtual impedance at the event of the fault proportional to the size of the magnitude of the fault current. The magnitude of the fault current is set to exceed a threshold value in order to activate this current limiting strategy, otherwise it will remain idle. The virtual impedance that is increased will cause a voltage command reduction which will in turn prevents overcurrent. The stator impedance adjuster block diagram is already presented in chapter 4, and it is included in this chapter considering the current-limiting capability.

From Fig. 5.7 b, L_{ls} represents the original virtual stator impedance, while L_{ls0} represents the constant virtual impedance that can be updated when the current-limiting control scheme is activated. As a result, L_{ls} becomes

$$L_{ls} = L_{ls0} + \Delta L_{ls} \tag{5.11}$$

This increased updated impedance reduces the peak current according to

$$V_{0M3C} = I_{max}(\omega L_{ls})^2 \tag{5.12}$$

where V_{0M3C} is the M3C voltage magnitude during the fault and I_{max} is the result maximum current allowed. L_{ls} is increased by adding the term ΔL_{ls}. The last value is determined from

$$\Delta L_{ls} = max\{k_z(i_{o,rms} - i_{thres}), 0\} \tag{5.13}$$

where k_z is the limiting factor, and *X/R* is the current limiting factor. The current limiter control strategy applied to the VSG control uses the amount of the overcurrent in order to generate additional output impedance. The control will provide a current limiting strategy in order to suppress the remote ac grid side output current, in which if it is not suppressed (not to exceed 2 pu), it will result in large reactive power generation (losses) as well as large frequency deviation.

In order to set the value of the tuning factor k_z, the tuning technique is used in [11], [13] which depends on the magnitude of the voltage drop V_{0M3C}. As explained in [13], it is complicated to determine k_z based on the desired voltage drop magnitude as each existed disturbance differs in nature, dynamics and its resulted voltage drop. For instance, from the frequency point of view and current limiting point of view, if the gain k_z is too small, the current limiting ability as well as the fault ride through ability will not succeed. On the other hand, if the gain is too high, it will create a robust current limiting ability but the system will suffer from a large frequency fluctuation, which is not acceptable considering the main target of the proposed dual VSG control scheme, which is to regulate ac side frequency.

5.5 Simulation Results

To verify the proposed system, several simulation tests were carried out in PSCAD/EMTDC software environment for the system shown in Fig. 5.2.

M3C 2 regulates the active power received from the main grid and sends this power through a 200 km LFAC link to M3C 1 by integrating the virtual mechanical speed from the VSG to provide the phase angle. Then the LFAC side VSG control of M3C 1 regulates the active power and uses its AVR to maintain the voltage by varying the reactive power. The remote ac grid includes a conventional SG and associated loads, which represents a relatively weak system. The fixed load P_{L1}+Q_{L1} is 400 MW + 100 Mvar, whereas a disturbance load $P_{L2} + Q_{L2}$ represents 5% of the fixed load and it is set to be turned on and off at specific times. These loads are being supplied by both SG and the M3C-LFAC system. The M3C 1 parameters and

the SG parameters are listed in Tables 5.1, and 5.2, respectively. On the other hand, the operation of the system under conventional control is explained in [1], as discussed in Section III-B.

The SG is built by using transient and sub-transient parameters of a round rotor type obtained from [14], [15]. The conventional SG control is shown in Fig. 5.8. It consists of three parts, the AVR, the speed governor, and the load frequency control (LFC). The LFC is needed to regulate frequency deviations due to active load dynamic variations.

The corresponding block diagram of frequency regulation is shown in Fig. 5.8(a), where T_G represents the time constant of the speed governor and F_{HP}, T_{RH} and T_{CH} are the coefficients of the reheat turbine [16]. These parameters values are given in Table 5.2. The output of this controller is the input set point of the mechanical torque (T_m) used for the SG. The AVR shown in Fig. 5.8(b) is employed to maintain the output voltage.

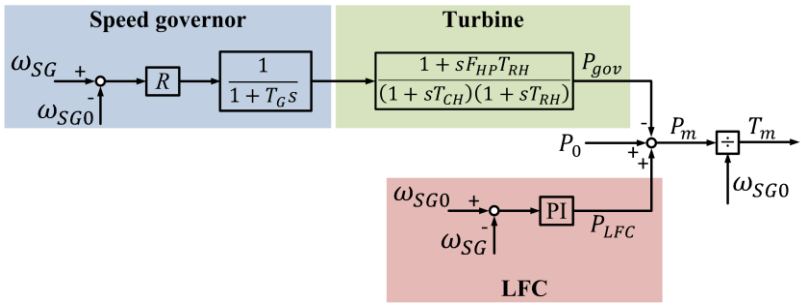

(a)

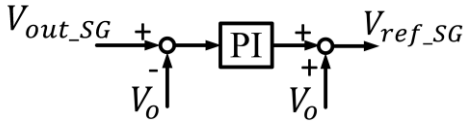

(b)

Fig. 5.8 Control block of Synchronous Generator; (a) speed governor, turbine model, and Load Frequency Control (LFC), and (b) Automatic Voltage Regulator (AVR) block

Table 5.1 Simulation Parameters of M3C 1

Common Parameters	
Parameter	Value
Rater M3C Power	200 MVA
$V_{base\ LFAC}$	275 kV
$V_{base\ grid}$	150 kV

f_{LFAC}	10 Hz
f_{grid}	60 Hz
X_{grid}	0.1 pu
X_{LFAC}	0.016 pu

M3C Internal Parameters	
Parameter	Value
Sampling Frequency	2 kHz
Capacitor Voltage	128 kV
Cell Capacitor	0.69 s
Arm Inductor	0.008 pu

Q-V droop and AVR PI Controllers Parameters	
Parameter	Value
K_p	0.2 s
K_i	0.5 s
K_{q_pu}	10 pu

Stator Impedance Adjuster and Current Limiter Parameters	
Parameter	Value
LFAC side L_{lso}	0.541 pu
Grid side L_{lso}	0.569 pu
k_z	1

VSG Parameters		
	LFAC side	Grid side
Parameter	Value	Value
V_{base}	275 kV	275 kV
$P_{0_{pu}}$	1 pu	1 pu
ω_0	62.8315 rad/s	376.9911 rad/s
M	8 s	8 s
$k_{p_{pu}}$	20 pu	20 pu
$k_{v_{ave_{pu}}}$	10 pu	-
T_f	0.0159 s	0.00265 s
k_{xp}	1	1

$k_{x\omega}$	91.4140 pu	202.1987 pu
k_{xi}	8.8522 s^{-1}	23.4591 s^{-1}

Table 5.2 Simulation Parameters of Round Rotor SG

Parameter	Value
Rated S_{SG}	200 MVA
Terminal voltage	13.8 kV
M	3.2 s
x_d, x'_d, x''_d	1.65, 0.23, 0.17
x_q, x'_q, x''_q	1.59, 0.38, 0.17
$\tau'_d, \tau''_d, \tau''_q$	0.83, 0.023, 0.023
Stator resistance R_s	2.8544 e-3 pu
Governor droop coefficient R	20 pu
LFC PI controller time constant	0.5 s
Speed governor coefficient T_G	0.1 s
Turbine HP coefficient F_{HP}	0.3 s
Time constant of reheater T_{RH}	7.0 s
Time constant of main inlet volumes T_{CH}	0.2 s

Case 1: Load Change Scenario

Generally, in the frequency regulation point of view, the most common disturbance in power system is load change [17]. If the power system lacks the inertia, this will lead to a large frequency deviation. This deviation, particularly if the load varies significantly, may lead to system instability.

Figs. 5.9 and 5.10 show the simulation results for a step load increase and decrease, respectively. In order to perform the load change, a switchable load P_{L2}+Q_{L2} as can be seen from Fig. 5.2, is turned on or off, at t = 20 s, to perform load increase or decrease. Fig. 5.9(a) illustrates the SG rotor angular frequency. It can be observed that when the system is under the VSG control, the frequency nadir is reduced, and the frequency fluctuation becomes slower and smoother than that under the conventional control. After a short period of transient (which is decided by the LFC controller of the SG), the frequency of the grid can be restored to the nominal value. Thus, the VSG has improved system stability.

Figs. 5.9(b), (c), and (d) illustrate the active powers of the SG, and the M3C in both grid and LFAC sides, respectively. It can be noticed that the VSGs of both grid side and LFAC side are reacting in order to inject power into the remote ac grid to support the load increase demand. This confirms how the M3C-

LFAC link can provide fast power injection response. From Fig. 5.9(c), it is clear that the M3C injects the required power until the SG increases its active power as shown in Fig. 5.9(b) to respond to the power mismatch. Similarly, the VSG on the LFAC side will request this power to be provided from M3C 2 through LFAC link. As a result, both VSGs respond accordingly to inject the required power. Once the steady-state operation is restored, the M3C-LFAC system restores its active power to the pre-transient value. It can be confirmed that all VSGs have enhanced the M3Cs with a fast response to support the frequency regulation of the remote ac grid.

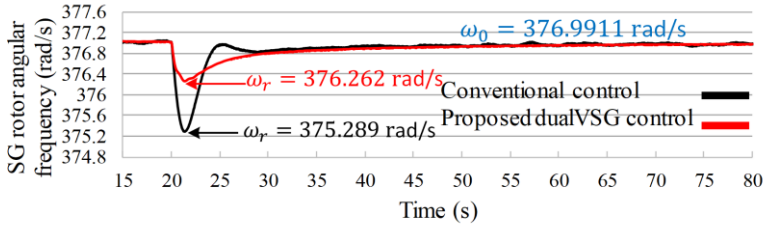

(a)

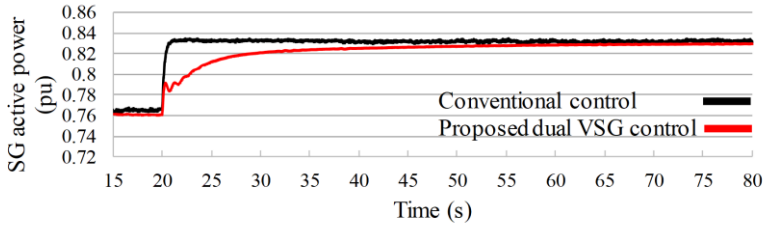

(b)

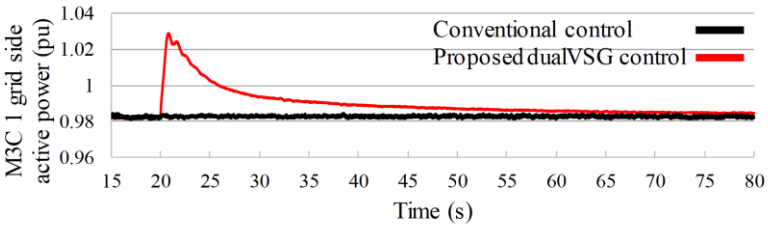

(c)

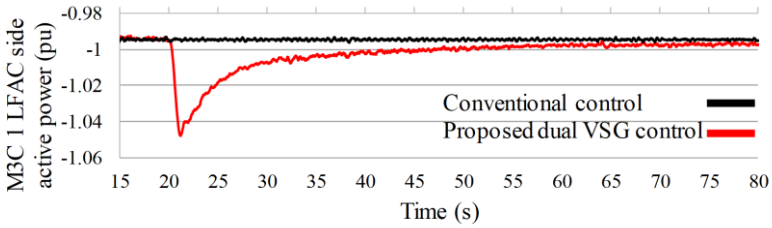

(d)

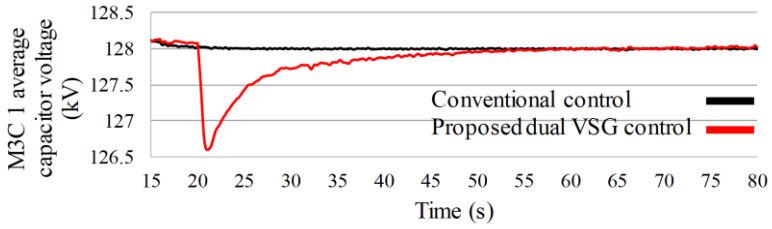

(e)

Fig 5.9 Simulation waveforms of the system with the proposed dual VSG control and with conventional control under 5% load increase: (a) SG rotor angular frequency, (b) SG active power, (c) M3C 1 grid side active power, (d) M3C 1 LFAC side active power, and (e) M3C 1 average dc capacitor voltage.

Fig. 5.10 shows the simulation results of the step load decrease scenario. This scenario is initiated by turning off the switchable load. As the case of step load increase, the VSG controller has succeeded in mitigating the frequency deviation as shown in Fig. 5.10(a). Figs. 5.10(b), (c), and (d), show the active powers of the SG, and M3C 1 grid and LFAC sides, respectively. Again, the VSG controls on both sides allow the M3C-LFAC system to respond fast to support this load reduction, compared with the conventional control that does not allow the M3C to have an inertial response.

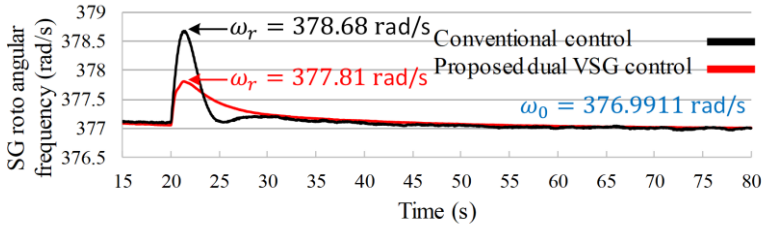

(a)

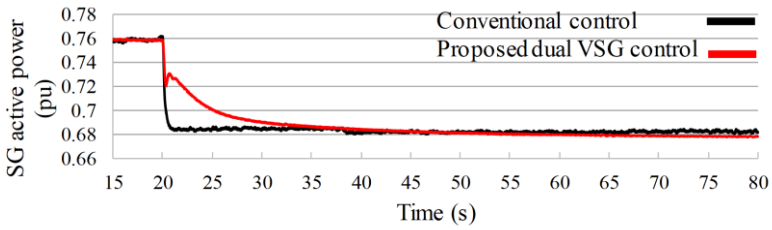

(b)

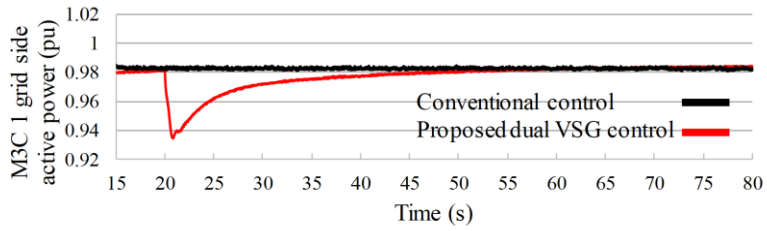

(c)

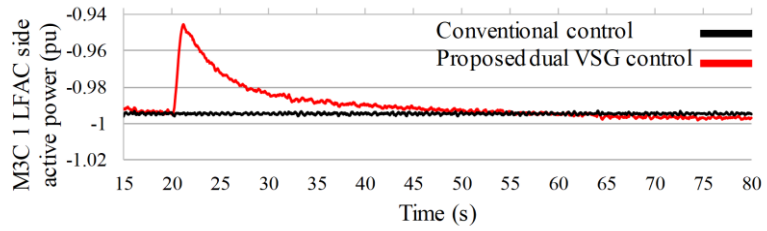

(d)

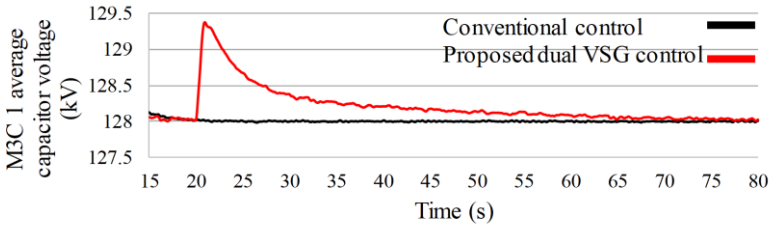

(e)

Fig. 5.10 Simulation waveforms of the system with the proposed dual VSG control and with conventional control under 5% load decrease: (a) SG rotor angular frequency, (b) SG active power, (c) M3C 1 grid side active power, (d) M3C 1 LFAC side active power, and (e) M3C 1 average dc capacitor voltage.

In both load change scenarios, the VSG control has succeeded in mitigating the frequency deviation and the average dc capacitor voltage deviation is kept within 2% during transient states. Moreover, from Figs. 5.9(e) and 5.10(e), the proposed V_{ave}-P droop on the LFAC side managed to maintain the power balance between the input and the output and thus, succeeded in keeping the average dc capacitor voltage constant.

Case 2: Three Phase-to-Ground Fault Scenario

Fig. 5.11 shows a performance comparison of the M3C-LFAC system interconnecting a remote ac grid with the proposed dual VSG-based control and conventional control schemes during a fault event. A three-phase-to-ground fault (with a grounding resistance of $R_G = 5\ \Omega$) located at the load referring to Fig. 5.2, is initiated at t = 15 s and cleared at t = 15.5 s by opening the faulty line. Then, a first successful reclosing attempt of a circuit breaker after the fault is cleared at t = 15.7 s (according to a typical reclosing time of an SF_6 circuit breaker [18]) occurred to bring back the line in operation.

From Fig. 5.11(e), the fault causes a voltage drop of about 75 % at the remote ac grid side of M3C 1. From Fig. 5.11(a), it is depicted that when the fault occurs, under the proposed dual VSG control with stator-impedance-based current limiting, the SG rotor angular frequency variation is mitigated compared with the conventional control. From Figs. 5.11(b), and 5.11(c), it can be seen that the VSG control enables SG and M3C 1 to maintain the power variation not to exceed 0.5 pu. On the other hand, the performance of the conventional control is not favorable, which results in large power oscillation.

Moreover, the VSG control was further enhanced to include a fault ride-through capability owing to the current limiter control scheme embedded in the stator impedance adjuster block. When the fault occurs, the control scheme is able to perform a current-limiting strategy. There is a trade-off between suppressing the fault current and the frequency deviation. It is well known that a more suppressed current results in a larger frequency deviation. Therefore, from the frequency support point of view, the current is maintained at 2 pu in order to show the frequency support property of the proposed controller compared with the conventional control. On the other hand, with the conventional control, the strategy on limiting the fault current is inherited from the same strategy used with inverter-based DGs using a multi-loop control [13], by limiting the references dq components of the inner and outer conventional controller loops. However, the investigation on the M3C with conventional control taking into account the occurrence of fault as a case study is still immature and requires further study. As can be seen in Fig. 5.11(d), the conventional control fails to limit the overcurrent within an acceptable value. The limiters of the conventional control were set to 1.06 pu. Thus, without altering the conventional control, the advantages of the proposed dual

VSG control scheme are targeted, in this case, to provide a fault ride-through capability as well as providing the remote ac grid with dynamic frequency support.

Generally, the M3C-LFAC link based on the proposed dual VSG control strategy is more effective in increasing the system inertia, providing prompt frequency support, and thus reducing frequency deviation of low inertia grid.

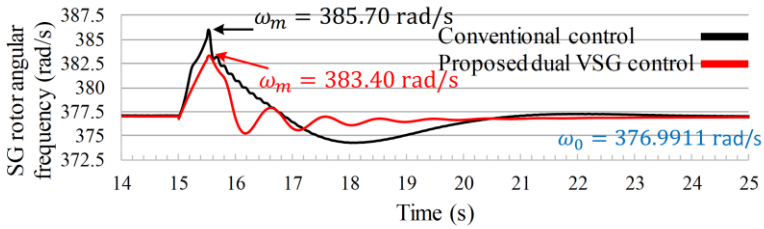

(a)

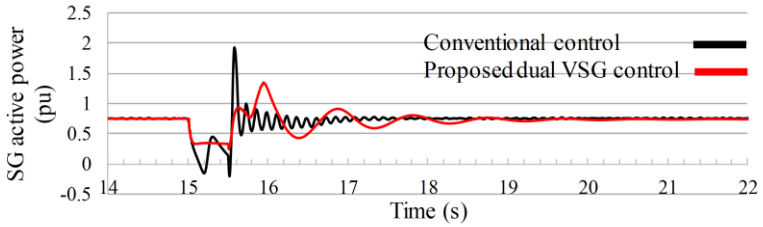

(b)

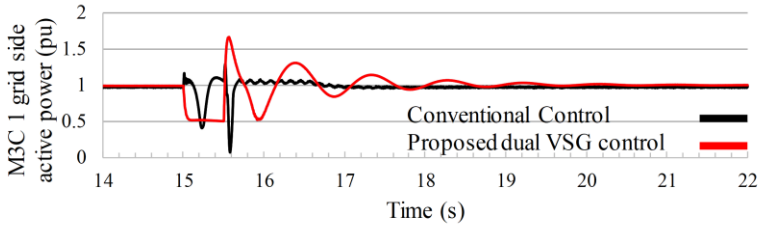

(c)

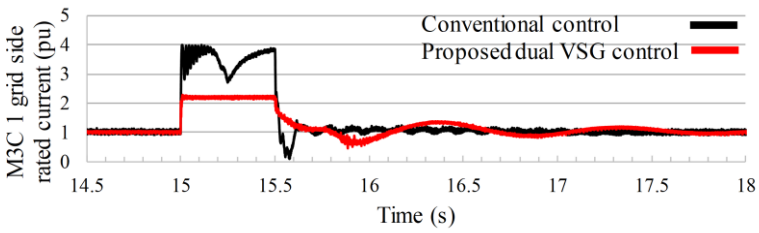

(d)

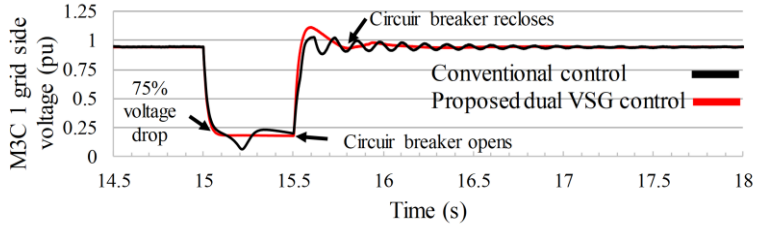

(e)

Fig 5.11 Simulation waveforms of the system with VSG control and with conventional control under 500-ms three-phase-to-ground ($\boldsymbol{R_g = 5\Omega}$) fault at the load: (a) SG rotor angular frequency, (b) SG active power , (c) M3C 1 grid side active power, (d) M3C 1 rated current, and (e) M3C 1 grid side voltage amplitude.

5.6 Summary

This chapter provides a frequency regulation support scheme during transients to a remote ac grid. This control scheme is proposed for the M3C-LFAC system by applying a dual VSG control at the remote ac grid side M3C 1. The VSG control strategies applied to both sides of this M3C can enable both sides of the M3C to behave stably by providing virtual inertia.

From the frequency support point of view, the increased inertia can enhance the dynamic performance of a small rating remote ac grid. Moreover, on the LFAC side, the VSG control is applied to autonomously control active power and maintain the frequency stable in the steady-state. In order to address the difficulty of H-bridge cell dc capacitor average voltage regulation introduced by the dual VSG control scheme, V_{ave}-P droop control is incorporated in the LFAC side VSG control.

The effectiveness of the proposed dual VSG control strategy for the M3C-LFAC system is demonstrated by the time-domain simulation studies performed in the PSCAD/EMTDC software environment. It is shown that the proposed control scheme significantly outperforms its conventional counterpart.

References

[1] M. Al-Tameemi, Y. Miura, J. Liu, H. Bevrani, and T. Ise, "A novel control scheme for multi-terminal low-frequency ac electrical energy transmission systems using modular multilevel matrix converters and virtual synchronous generator concept," *Energies*, vol. 13, no. 3, 747, Feb. 2020.

[2] M. Guan, W. Pan, J. Zhang, Q. Hao, J. Cheng, and X. Zheng, "Synchronous generator emulation control strategy for voltage source converter (VSC) stations," *IEEE Trans. Power Syst.*, vol. 30, no. 6, pp. 3093–3101, Nov. 2015.

[3] Y. Miura, T. Mizutani, M. Ito, and T. Ise, "Modular multilevel matrix converter for low frequency AC transmission," in *Proc. 2013 IEEE 10th Int. Conf. Power Electron. Drive Syst*., 2013, pp. 1079–1084.

[4] W. Kawamura, K.-L. Chen, M. Hagiwara, and H. Akagi, "A low-speed, high-torque motor drive using a modular multilevel cascade converter based on triple-star bridge cells (MMCC-TSBC)," *IEEE Trans. Ind. Appl.*, vol. 51, no. 5, pp. 3965–3974, Sept./Oct. 2015.

[5] J. Liu, Y. Miura, and T. Ise, "Fixed-parameter damping methods of virtual synchronous generator control using state feedback," *IEEE Access*, vol. 7, pp. 99177–99190, 2019.

[6] T. Shintai, Y. Miura, and T. Ise, "Oscillation damping of a distributed generator using a virtual synchronous generator," *IEEE Trans. Power Del*., vol. 29, no. 2, pp. 668–676, Apr. 2014.

[7] J. Liu, Y. Miura, H. Bevrani, and T. Ise, "Enhanced virtual synchronous generator control for parallel inverters in microgrids," *IEEE Trans. Smart Grid*, vol. 8, no. 5, pp. 2268-2277, Sept. 2017.

[8] J. Liu, Y. Miura, and T. Ise, "Comparison of dynamic characteristics between virtual synchronous generator and droop control in inverter-based distributed generators," *IEEE Trans. Power Electron.*, vol. 31, no. 5, pp. 3600–3611, May 2016.

[9] K. Sakimoto, Y. Miura, and T. Ise, "Stabilization of a power system including inverter type distributed generators by the virtual synchro-nous generator," *Electrical Engineering in Japan*, vol. 187, no. 3, pp. 7–17, May 2014 [Translated from *IEEJ Trans. Power and Energy*, vol. 132, no. 4, pp. 341–349, Apr. 2012 (in Japanese)].

[10] T. Ngo, M. Lwin, and S. Santoso, "Steady-state analysis and performance of low frequency ac transmission lines," *IEEE Trans. Power Syst.*, vol. 31, no. 5, pp. 3873–3880, Sept. 2016.

[11] A. D. Paquette and D. M. Divan, "Virtual Impedance Current Limiting for Inverters in Microgrids With Synchronous Generators," in *IEEE Transactions on Industry Applications*, vol. 51, no. 2, pp. 1630-1638, March-April 2015.

[12]J. Liu, Y. Miura, and T. Ise, "Power Quality improvement of microgrids by virtual synchronous generator control," in *Proc. Elect. Power Quality Supply Rel. Conf. (PQ)*, Tallinn, Estonia, 2016, pp. 119–124.

[13]J. Jongudomkarn, J. Liu, and T. Ise, "Virtual synchronous generator control with reliable fault ride-through ability: a solution based on finite-set model predictive control," *IEEE J. Emerg. Sel. Topics Power Electron.*, to be published, doi: 10.1109/JESTPE.2019.2942943.

[14]J. Machwiski, J. W. Bialek, and J. R. Bumby, *Power System Dynamics Stability and Control*, 2nd Ed. Chichester, UK: John Wiley & Sons, 2008.

[15]J. Fang, H. Li, Y. Tang, and F. Blaabjerg, "Distributed power system virtual inertia implemented by grid-connected power converters," *IEEE Trans. Power Electron.*, vol. 33, no. 10, pp. 8488–8499, Oct. 2018.

[16]P. Anderson and A. A. Fouad, *Power System Control and Stability*. Ames, IA, USA: Iowa State Univ. Press, 1977.

[17]H. Bevrani, *Robust Power System Frequency Control,* 2nd ed. New York, NJ, USA: Springer, 2014.

[18]*Network Protection & Automation Guide*, 3rd ed. May 2011. Paris, France: Alstom Grid, 2011.

Chapter 6
Conclusions

6.1 Research Summary and Achievements

In this dissertation, the Low Frequency AC (LFAC) system driven by a Modular Multilevel Matrix Converter (M3C)-based Virtual Synchronous Generator (VSG) control was established to form a different M3C-LFAC system configurations aiming at different applications.

In chapter 2, a review of the related technologies associated with this study is described. A brief survey includes a comparison of these techniques with alternative ones, such as:

1- Comparing the LFAC system with High Voltage AC (HVAC) and High Voltage DC (HVDC) systems.
2- Describing the M3C configuration and its existed control methods.
3- The basics of VSG control and its applications.
4- To show the transmission distance extension capability of the LFAC system.
5- The M3C succeeded at performing frequency conversion in high ratings with improved power quality and low power conversion losses.

In chapter 3, a point-to-point LFAC system is built using M3C based on conventional and VSG controls. This work aimed at showing the synchronized power feature of the VSG control. This establishment is essential to open a wide door for future potential applications.

In chapter 4, a novel multiterminal LFAC (MT-LFAC) system is constructed using M3C-based VSG control. Each part has its own contribution:

1- The VSG has succeeded in enabling each M3C in the MT-LFAC system to behave like an SG.
2- The applications of the VSG successfully maintained the steady-state frequency
3- The issue of the low *X/R* ratio in the LFAC system is solved by equipping a stator impedance adjuster control.
4- Autonomous frequency restoration is realized by proposing a frequency restoration mode control scheme for the governor part of the VSG control.

As a result, the MT-LFAC system using the proposed technology has proved its flexibility and its ease of implementation.

In chapter 5, another application is proposed to validate our system. The M3C-LFAC system is extended to aid the large frequency deviation issue of a small rating remote ac grid. The LFAC using VSG control

for the M3C is able to regulate frequency, and thus, can be considered a competitive alternative solution considering the existing limitations of the HVDC system. A dual VSG control is implemented for the M3C control which replaced the conventional control. The implementation of the dual VSG controller has added a new property to the system in which the M3C is now showing an inherited and a dual inertial and frequency response from input and output sides.

6.2 Future Research Steps

1- To investigate the effectiveness of the proposed control scheme and to minimize the existing gap between simulation environment and practice, in the present research, the detailed dynamics for the system under study are considered, and high precise nonlinear models for the components and accurately defined parameters in the proposed control framework are employed. However, since the experimental test is the ultimate approach for validation of a new control strategy, this issue can be considered to be a future step for the present research work. Further research steps can be focused on coordination control of M3C with AC grids in order to reduce the impact on AC grids, and evaluation of losses of the system are considered.

2- In this study, the operating frequency is selected to be 10 Hz, however, such lowered frequency results in increasing the weight and the footprint of the low-frequency transformer as well as the M3C sub-module capacitor. Meanwhile, increasing the frequency to the 60/3 Hz will result in increasing the charging current and reducing the transmission length. Therefore, investigation on choosing the optimal operating frequency is required as well as designing a low-frequency transformer as well as sub-module capacitor within the acceptable footprint and weight must be taken into account in future work.

List of Publications

Journal Publications (with review)

1- Mustafa Al-Tameemi, Yushi Miura, Jia Liu, Hassan Bevrani, and Toshifumi Ise, “A Novel Control Scheme for Multi-Terminal Low-Frequency AC Electrical Energy Transmission Systems Using Modular Multilevel Matrix Converters and Virtual Synchronous Generator Concept”. *Energies (MDPI)*, 2020, Vol. 13, Issue 3, No. 747; doi.org/10.3390/en13030747, pp. 1-19, February 2020.

2- M. Al-Tameemi, J. Liu, H. Bevrani and T. Ise, "A Dual VSG-Based M3C Control Scheme for Frequency Regulation Support of a Remote AC Grid Via Low-Frequency AC Transmission System," in *IEEE Access*, vol. 8, pp. 66085-66094, 2020, DOI: 10.1109/ACCESS.2020.2985386.

Papers Presented at International Conferences (Oral presentation, with review)

1- Mustafa Al-Tameemi, Yushi, Miura and Toshifumi Ise, “Low Frequency AC Transmission System using Modular Multi Level Matrix Converter with Virtual Synchronous Generator Control”, in Proceedings of *the International Conference on Electrical Engineering (ICEE 2018)*, Korea University, Seoul, South Korea, 2018, pp. 1-6.

Acknowledgements

First and foremost, praises and thanks to God, the Almighty, for His showers of blessings throughout my research work and my life. Undertaking this PhD has been a truly life-changing experience for me and it would not have been possible to do without the help of God who put many people in my life who supported and guided me throughout this journey.

I would like to express my deep and sincere gratitude to my research supervisors Shigemasa Takai and Professor Toshifumi Ise, in the Graduate school of Engineering, Osaka University, for their continuous guidance, persistent help of my PhD study. I also would like to give my appreciation to Prof. Yushi Miura for his insightful advice and his big heart. Special thanks must also go to Dr. Jia Liu, assistant professor at the Graduate School of Engineering, Osaka University, who guided me tirelessly from the very beginning. His kindness, technical insights, and experience were essential, and his attitude made the entire research process a more informative and enjoyable experience.

Besides, I would like to express my thanks to the other members of my dissertation committee: Professor Tsuyoshi Funaki, Professor Tomoo Ushio, Professor Hiroyuki Shiraga, and Invited Professor Shigekazu Sakabe in the Graduate School of Engineering, Osaka University, for their valuable comments and encouragement, and for their challenging questions, which incented me to widen my research from various perspectives.

I would like to extend my sincere gratitude to Professor Hassan Bevrani in the Department of Electrical Engineering, University of Kurdistan, Iran, for his helpful advice on my researches and constructive guidance, especially during the revision of my published articles as well as the manuscript.

I would like to express my thanks to other staff at Osaka University for their help and supports during the doctoral course study.

I would like to present my most sincere gratitude to the Japanese Ministry of Education, Culture, Sports, Science and Technology, for giving me a great opportunity to study in Japan and for granting me the MEXT scholarship.

My deepest appreciation to the staff of the National Institute of Biomedical Innovation, Health and Nutrition (NIBIOHN). Especially Nomura Project team members: Prof. Nomura Taisei, Prof. Ryo Haruko, Adachi Shigeki Sensei, Hatanaka Eiko, Yasuda Kou Joon, Enomoto Kumiko. For their support and kindness during my study.

Outside the university, my daily life would have been more difficult if I wouldn't have my host mother Toshiko Nishikawa who was and been always beside me and my family. I am grateful and in debt to her for the rest of my life.

I am extremely grateful to my parents for their love, prayers, caring and sacrifices for educating and preparing me for my future. I also would like to express my love to my younger sisters, and younger brother, for their support and continuous belief in me. In the end, I am very much thankful to my wife Lobna and my son Yaseen for their love, sacrifice, prayers and continuing support to complete this research work.